REPORT DOCUMENTATION PAGE

Form Approved OMB NO. 0704-0188

1. REPORT DATE (DD-MM-YYYY)	2. REPORT TYPE	3. DATES COVERED (From - To)
	New Reprint	-

4. TITLE AND SUBTITLE

A Classical Trajectory Study of the Dissociation and Isomerization of C2H5

5a. CONTRACT NUMBER
W911NF-09-1-0199

5b. GRANT NUMBER

5c. PROGRAM ELEMENT NUMBER
611102

6. AUTHORS

Albert F. Wagner, Luis A. Rivera-Rivera, Damien Bachellerie, Jamin W. Perry, Donald L. Thompson

5d. PROJECT NUMBER

5e. TASK NUMBER

5f. WORK UNIT NUMBER

7. PERFORMING ORGANIZATION NAMES AND ADDRESSES

University of Missouri - Columbia
Office of Sponsored Programs
The Curators of the University of Missouri
Columbia, MO 65211 -3020

8. PERFORMING ORGANIZATION REPORT NUMBER

9. SPONSORING/MONITORING AGENCY NAME(S) AND ADDRESS(ES)

U.S. Army Research Office
P.O. Box 12211
Research Triangle Park, NC 27709-2211

10. SPONSOR/MONITOR'S ACRONYM(S)
ARO

11. SPONSOR/MONITOR'S REPORT NUMBER(S)
56225-EG.2

12. DISTRIBUTION AVAILIBILITY STATEMENT

Approved for public release; distribution is unlimited.

13. SUPPLEMENTARY NOTES

The views, opinions and/or findings contained in this report are those of the author(s) and should not contrued as an official Department of the Army position, policy or decision, unless so designated by other documentation.

14. ABSTRACT

Motivated by photodissociation experiments in which non-RRKM nanosecond lifetimes of the ethyl radical were reported, we have performed a classical trajectory study of the dissociation and isomerization of C2H5 over the energy range 100–150 kcal/mol. We used a customized version of the AIREBO semiempirical potential (Stuart, S. J.; et al. J. Chem. Phys.2000, 112, 6472–6486) to more accurately describe the gas-phase decomposition of C2H5. This study constitutes one of the first gas-phase applications of this potential form. At each energy, 10?000

15. SUBJECT TERMS

AIREBO, Isotopic Scrambling, Ethyl Radical, Semi-empirical PES, Kinetic Models

16. SECURITY CLASSIFICATION OF:			17. LIMITATION OF ABSTRACT	15. NUMBER OF PAGES	19a. NAME OF RESPONSIBLE PERSON
a. REPORT	b. ABSTRACT	c. THIS PAGE			Donald Thompson
UU	UU	UU	UU		19b. TELEPHONE NUMBER 573-882-0051

Report Title

A Classical Trajectory Study of the Dissociation and Isomerization of C2H5

ABSTRACT

Motivated by photodissociation experiments in which non-RRKM nanosecond lifetimes of the ethyl radical were reported, we have performed a classical trajectory study of the dissociation and isomerization of C2H5 over the energy range 100–150 kcal/mol. We used a customized version of the AIREBO semiempirical potential (Stuart, S. J.; et al. J. Chem. Phys.2000, 112, 6472–6486) to more accurately describe the gas-phase decomposition of C2H5. This study constitutes one of the first gas-phase applications of this potential form. At each energy, 10?000 trajectories were run and all underwent dissociation in less than 100 ps. The calculated dissociation rate constants are consistent with RRKM models; no evidence was found for nanosecond lifetimes. An analytic kinetics model of isomerization/dissociation competition was developed that incorporated incomplete mode mixing through a postulated divided phase space. The fits of the model to the trajectory data are good and represent the trajectory results in detail through repeated isomerizations at all energies. The model correctly displays single exponential decay at lower energies, but at higher energies, multiexponential decay due to incomplete mode mixing becomes more apparent. At both ends of the energy range, we carried out similar trajectory studies on CD2CH3 to examine isotopic scrambling. The results largely support the assumption that a H or a D atom is equally likely to dissociate from the mixed-isotope methyl end of the molecule. The calculated fraction of products that have the D atom dissociation is 20%, twice the experimental value available at one energy within our range. The calculated degree of isotopic scrambling is non-monotonic with respect to energy due to a non-monotonic ratio of the isomerization to dissociation rate constants.

REPORT DOCUMENTATION PAGE (SF298)
(Continuation Sheet)

Continuation for Block 13

ARO Report Number 56225.2-EG
A Classical Trajectory Study of the Dissociation ...

Block 13: Supplementary Note

Approved for public release; distribution is unlimited.

THE JOURNAL OF PHYSICAL CHEMISTRY A

Article

pubs.acs.org/JPCA

A Classical Trajectory Study of the Dissociation and Isomerization of C_2H_5

Albert F. Wagner

Argonne National Laboratory, Chemical Sciences and Engineering Division, Argonne, Illinois 60439, United States

Luis A. Rivera-Rivera, Damien Bachellerie, Jamin W. Perry, and Donald L. Thompson*

University of Missouri-Columbia, Department of Chemistry, Columbia, Missouri 65211, United States

ABSTRACT: Motivated by photodissociation experiments in which non-RRKM nanosecond lifetimes of the ethyl radical were reported, we have performed a classical trajectory study of the dissociation and isomerization of C_2H_5 over the energy range 100−150 kcal/mol. We used a customized version of the AIREBO semiempirical potential (Stuart, S. J.; et al. *J. Chem. Phys.* **2000**, *112*, 6472−6486) to more accurately describe the gas-phase decomposition of C_2H_5. This study constitutes one of the first gas-phase applications of this potential form. At each energy, 10 000 trajectories were run and all underwent dissociation in less than 100 ps. The calculated dissociation rate constants are consistent with RRKM models; no evidence was found for nanosecond lifetimes. An analytic kinetics model of isomerization/dissociation competition was developed that incorporated incomplete mode mixing through a postulated divided phase space. The fits of the model to the trajectory data are good and represent the trajectory results in detail through repeated isomerizations at all energies. The model correctly displays single exponential decay at lower energies, but at higher energies, multiexponential decay due to incomplete mode mixing becomes more apparent. At both ends of the energy range, we carried out similar trajectory studies on CD_2CH_3 to examine isotopic scrambling. The results largely support the assumption that a H or a D atom is equally likely to dissociate from the mixed-isotope methyl end of the molecule. The calculated fraction of products that have the D atom dissociation is ∼20%, twice the experimental value available at one energy within our range. The calculated degree of isotopic scrambling is non-monotonic with respect to energy due to a non-monotonic ratio of the isomerization to dissociation rate constants.

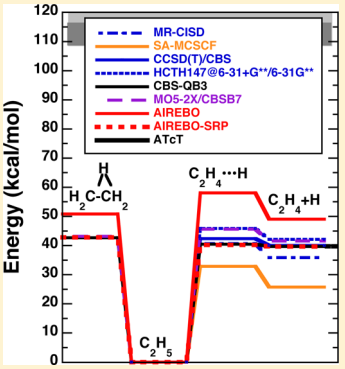

1. INTRODUCTION

The dissociation of the ethyl radical (C_2H_5) plays an important role in combustion chemistry. Because the reverse reactions constitute the addition of a hydrogen atom to a stable molecule (as opposed to radical−radical recombination), the bond energies are relatively small. Consequently, this radical tends to dissociate rapidly in the primary reaction zones of premixed flames. The hydrogen atom thus produced acts to promote chain branching through the $H + O_2 \rightleftharpoons OH + O$ reaction. Thus, the rate coefficients for this dissociation, along with those of several other small radicals, are important factors in determining such global combustion properties as laminar flame speeds, induction times, and flammability, extinction, and ignition limits.[1,2]

Because of its importance in combustion, the thermal kinetics of ethyl radical dissociation has been studied for many years,[3] and the most recent reviews[4−6] show a consensus for the value of the thermal rate constant as functions of temperature and pressure. This consensus includes strong agreement between experiment and theory[7] for the dissociation kinetics.

In addition to thermal kinetics experiments, there have been several photoinduced dissociation experiments that access either the lower 3s Rydberg band[8−11] in C_2H_5 or the higher 3p band,[12] or both.[13] These experiments create ethyl radicals by photolysis or pyrolysis from some suitable precursor, activate the radical by photoabsorption of 260 to 193 nm light, and then photodetect the H atoms in various ways. Before describing the experimental results, a brief review of the experiments is useful. There are four potential sources of C_2H_5 in these experiments. The photoabsorption[8,9,12] of the ethyl radical places it in a Rydberg state from which a H atom can directly dissociate adiabatically, leaving behind an excited C_2H_4. The H atom can also migrate between the carbon atoms, passing through a conical intersection to the ground electronic state. (Theoretical calculations of reaction paths on the electronically excited-state potential energy surfaces (PESs) of C_2H_5[14] predict that the nonclassical bridge structure is a minimum on the 3s PES and a conical intersection to the ground state. The bridge structure is also a minimum in the 3p state but does not intersect with the ground state.) Once in the ground state, C_2H_5 can dissociate to

Special Issue: Curt Wittig Festschrift

Received: October 9, 2012
Revised: February 27, 2013

   dx.doi.org/10.1021/jp3099889 | *J. Phys. Chem. A* XXXX, XXX, XXX−XXX

a H atom and ground-state C_2H_4, either directly or indirectly after temporary residence in the well on the ground-state PES. A fourth source[8] of H atoms may come from the precursor that is a monosubstituted ethane where the substituent R is weakly bonded. The radical R can then attack the ethyl radical, form RH, and subsequently be photodissociated along with the ethyl radical. Alternatively, R itself can dissociate and its products can be subsequently photodissociated. While the characteristics of the dissociated H atoms from all four sources are of intrinsic dynamical interest, the only source of particular relevance to combustion is the unimolecular dissociation on the ground electronic state surface.

Only the experiments on the 3s Rydberg band of the ethyl radical have produced results characteristic of a slow unimolecular dissociation of the radical. The experimental results (including a lack of consensus on certain points) may be summarized as follows:

(1) ~80% of photoexcited C_2H_5 dissociates by the unimolecular process.[9] However, Zierhut et al.[10] found only a fast (20 fs) decay of C_2H_5, which indicates direct dissociation; they did not observe a slower dissociation that could involve an intersystem crossing. This interpretation assumes that vibrationally excited C_2H_5 on the ground state surface lives long enough to be photoionized and subsequently detected by mass spectroscopy. Recently, Steinbauer et al.[11] confirmed the existence of both a unimolecular and direct dissociation channel.

(2) The differential cross section for that unimolecular decay is isotropic,[9] consistent with an excited complex that lasts at least a rotational period (~1 ps).

(3) The fraction of energy released into translation $\langle f_T \rangle$ is unexpectedly high from earlier work: 0.27 from ref 8 and 0.35 from ref 9. The most recent study[11] using velocity map imaging has $\langle f_T \rangle = 0.19$ for H atoms produced by the slow unimolecular process. This study suggests several experimental issues that could account for the higher values of earlier studies. The earliest study[8] characterized the translational energy distribution as Maxwellian. Subsequent studies have shown a bimodal distribution of translational energy of the H atoms due to direct and indirect dissociation. Decomposition of the distribution shows a low energy distribution that is Maxwell-like but is well represented by a more involved distribution.[11]

(4) The unimolecular dissociation rate is multiexponential with a slow component of 10^6–10^7 s^{-1} depending on the photon energy.[8,11] Rice–Ramsperger–Kassel–Marcus (RRKM) calculations[8] for the energy range of the experiment predict a rate of 10^{12} s^{-1}. The 5 orders of magnitude difference in the statistical theory rate and the measured rate is quite surprising and of course suggests nonstatistical behavior at very high energies. This slow rate is derived from the measured temporal growth and decay (due to diffusion out of the laser focus) of H atoms over ~400 ns. The measurements that produce these slow rates do not have the time resolution to observe picosecond decay rates. Thus, these measurements can only be interpreted to mean that there is a component of unimolecular decay many orders of magnitude slower than that predicted by RRKM.

Additional experimental results for isotopic scrambling are available. C_2H_5 can both dissociate and isomerize (i.e., undergo a 1–2 hydrogen shift):

$$H_2CCH_3 \rightarrow H_2CCH_2 + H \quad (1a)$$

$$H_2CCH_3 \rightleftharpoons H_3CCH_2 \quad (1b)$$

The isomerization process (eq 1b) is only detectable through isotopic scrambling:

$$D_2CCH_3 \rightarrow HD_2CCH_2 \rightarrow HDCCH_2 + D \quad (2)$$

The earliest photodissociation experiment[13] that accesses the 3s Rydberg band found some isotopic scrambling by detecting for CD_2CH_3 one D atom for every three H atoms. However, this early experiment used 193 nm light to photodissociate the precursor and that could contaminate the measured isotopic ratio. Two subsequent photodissociation[8,9] experiments that access this band did not detect any isotopic scrambling; however, the most recent experiment[11] did detect isotopic scrambling at a level of no more than 10%. All experiments[12,13] that directly access the 3p Rydberg band show isotopic scrambling that is attributed to isomerization on the excited state surface.[12] In a thermal dissociation experiment[15] of CD_2CH_3 and CH_2CD_3 over the temperature range from ~700 to ~1200 K, only the majority isotope was detected as the atomic dissociation product. The earliest but indirect scrambling study[16] involved D_3CCH_3 pyrolysis in which it was argued that product distributions require that isomerization be ~20% of the dissociation rate. It would appear that the current consensus is that, on the ground state PES, isomerization is at best a minor process relative to dissociation at both thermal and photoexcitation levels of energy.

The history of theoretical studies[17−23] relevant to the dynamics of C_2H_5 on the ground state PES mostly precedes all the photodissociation methods by several decades. The earliest trajectory studies by Hase's group using analytical[17,19,20] PESs based on *ab initio* electronic structure calculations found at higher energies (>100 kcal/mol) that unimolecular decay is described by a single rate constant well represented by statistical theories and of the order of 10^{12} s^{-1}. Their computed product translational energy distribution has the average value $\langle f_T \rangle = 0.18$. Isomerization was rarely observed in the trajectories, not surprising since the isomerization barrier is ~20 kcal/mol higher than the dissociation barrier on their PES[17] and isomerization was restricted to only one of the H atoms.[17] Later, electronic structure theory calculations[24] predicted this barrier to be only 5.0 kcal/mol above the dissociation barrier. Hase and co-workers[21] subsequently used high quality *ab initio* results and transition state theory calculations to obtain good agreement with measured thermal rate constants for dissociation and addition. This series of calculations are either consistent or unrelated to the photodissociation experimental results with the exception of providing no evidence for a very slow component to the unimolecular decay.

After the measured results of Gilbert et al.[8] of the slow decay, three different direct dynamics trajectory studies[25−27] have been carried out by the Chen group to understand the implications of the measurements. Two of those studies[25,26] were carried out at the HCTH147@6-31+G**/6-31G** level of theory (see the Glossary for details of this functional). Those two studies found biexponential decay that they associated with trapped, quasi-periodic trajectories (slow rate) in a sea of chaotic trajectories (fast rate). A wavelet-based analysis[28] was used to identify specific ethyl vibrational modes involved in the quasi-periodic motion. The third study[27] involved surface-hopping trajectories propagated on the multiple electronic states involved in the photoabsorption process. State-averaged

dx.doi.org/10.1021/jp3099889 | J. Phys. Chem. A XXXX, XXX, XXX–XXX

multiconfiguration self-consistent field (SA-MCSCF) and multireference configuration interaction with singles and doubles (MR-CISD) methods had to be used to provide a balanced description of both ground and excited electronic state PESs. This study found that only 13−25% of the originally excited ethyl radicals underwent indirect unimolecular dissociation on the ground or excited PESs. The study did find that those trajectories that underwent slow unimolecular decay on the ground state surface had a largely isotropic distribution, had a $\langle f_T \rangle$ of 0.24, had a single unimolecular dissociation rate of $\sim 0.5 \times 10^{12}$ s^{-1}, and isomerized on average ∼1.25 times. Although each trajectory typically isomerized at least once, the dissociated atom always started on the methyl end of the radical; in other words, no scrambling was observed even though isomerization occurred. This study is largely consistent with all the experimental measurements of unimolecular decay except for no discovery of a slow decay channel. The offered explanation is that slow decay is produced by trajectories trapped by the near resonance of vibrational frequencies. Such resonances can be strongly affected by curvature and anharmonicity changes produced by different electronic structure methods. Whether any of the three direct dynamics trajectory studies carried out by the Chen group are definitive enough to reliably describe resonances is open to question.

Of more practical concern, all three of the Chen group studies involved only hundreds of trajectories propagated on the ground state PES for at most 7 ps. (The surface hopping study comprised 5000 trajectories, but unimolecular dynamics on the ground state surface was only accessed by ∼15% of the trajectories. Relevant to the previous discussion of the four sources of H atoms in the experiment, this simulation suggests that the unimolecular dissociation is a minor channel.) Since the experimental observation is a 100 ns lifetime for the slow dissociation channel, the simulations are a factor of 10 000 too short to confirm experiment. Since only a small fraction of trajectories displayed the slow process, uncertainty from statistical sampling alone barely allows the slow process to be distinguished from the fast process over such a short time interval.

As discussed above, because of the inherent expense of direct dynamics, all of the theoretical studies designed to better understand the photoinduced ethyl radical dissociation experiments were based on too few trajectories of too short duration. There are only two ways to lift these restrictions. First, one can fit electronic structure calculations on the PES to a computationally inexpensive but accurate functional form and run more and longer trajectories with that form. Second, one can use an inexpensive semiempirical PES for the trajectory runs. We are interested in both approaches, and this article reports our results for the second approach.

Even with inexpensive PESs, running many trajectories for hundreds of nanoseconds is a formidable endeavor. In the present case, the dynamics is really the competition between two elementary processes (dissociation and isomerization) that can be readily defined and identified in the trajectories. This suggests that long-time dynamics could be followed by a kinetics model in which trajectories determine the rates of the elementary processes and the solution to the differential equations of the model determines the long-time behavior. There is another advantage to using a kinetics model. If the dynamics is fully statistical, then a kinetics model will display only one rate for product formation. However, if the dynamics is not fully statistical, then the rates of other processes, such as intramolecular vibrational redistribution (IVR) of energy, can influence the effective dissociation and/or isomerization rates. In such circumstances, kinetics models will display multiexponential behavior. In other words, the competition between dissociation and isomerization, as well as dissociation and/or isomerization by itself, can display how divided phase space is.

The rest of this paper describes a trajectory study in which 10 000 trajectories at several energies were followed up to 100 ps on a semiempirical PES. The trajectories where converted into "populations" of unisomerized C_2H_5, once isomerized C_2H_5, twice isomerized C_2H_5, etc. Various kinetics models are fit to the temporal behavior of the normalized populations. Both the trajectories themselves and the kinetics models are used to interpret the unimolecular dynamics. The rest of this article is organized as follows. In section 2, we describe the semiempirical PES and the computational details of the trajectories. In section 3, we present and discuss our trajectory results for six total energies that bracket the photon energies used in the experimental photodissociation studies of C_2H_5. In section 4, we derive various kinetics models that are used to analyze the trajectories. Section 5 includes a summary and a brief discussion of future work.

2. COMPUTATIONAL METHODS

2.1. PES and Level of Theory. There have been five previous[21,25,27] PESs derived from *ab initio* or semiempirical electronic structure calculations. The five sets of calculated energetics on the ground state PES are listed in Table 1, and four of the sets of energetics are displayed in Figure 1. The energy scale of the figure is expanded to include the energy range of the photodissociation experiments of Gilbert et al.,[8] Amaral et al.,[9] and Steinbauer et al.[11] (all in the darker band) and those of others[12,13] (the lighter band). Both the table and the figure show only classical results without zero point corrections. (Since quasi-classical trajectories are used to follow the dynamics, initial zero point energy is not retained by the trajectories during the unimolecular dissociation event. Consequently, displaying energetics without zero point corrections is most relevant to the trajectory dynamics

Table 1. C_2H_5 Energies in kcal/mol Calculated by the Listed Electronic Structure and Semi-Empirical Methods for the Isomerization and Dissociation Saddle Points, and the Dissociation Products (the Zero of Energy is the Energy of the Equilibrium Position of C_2H_5; the Bottom Row Gives the Experimental Dissociation Energy)

	H /\ H_2C-CH_2	C_2H_4•••H	$C_2H_4(^1S)$+H
Present Work			
CBS-QB3	42.7	40.5[a]	39.7
M05-2X/CBSB7	43.2	45.7	41.6
AIREBO	50.9	58.1	49.1
AIREBO-SRP	42.8	40.3	39.7
Past Work			
HCTH147@6-31+G**/6-31G**[b]		45.9	42.1
CCSD(T)/CBS[b]		42.4	40.1
QCISD(T)/6-311+G(2df,p)[c]		41.6	38.1
MR-CISD/6-31++G(d,p)[d]		40.7	35.9
SA-MCSCF/6-31++G(d,p)[d]		32.9	25.8
Experiment[e]			39.7[f]

[a]See ref 39. [b]References 25 and 31. [c]Reference 21. [d]Reference 27. [e]Reference 29. [f]Reference 30.

dx.doi.org/10.1021/jp3099889 | J. Phys. Chem. A XXXX, XXX, XXX−XXX

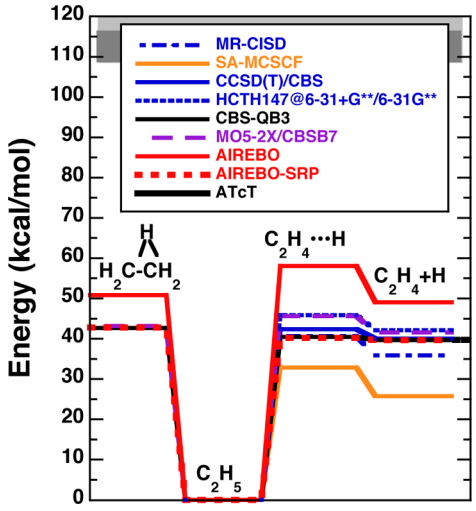

Figure 1. Calculated energetics diagram of C_2H_5 including both the dissociation and isomerization transition state and the dissociation asymptote. The different methods of calculation are described in the text. The one experimental result in the figure is labeled ATcT and is described in the text.

described in section 3.) The most recent experimental determination[29] of D_0 for $C_2H_5 \rightarrow C_2H_4 + H$ is 34.9 kcal/mol. For Figure 1, D_e was obtained from D_0 via high level anharmonic vibrational frequency calculations[30] (as the experimentally measured vibrational frequencies for C_2H_5 are incomplete) to obtain the 39.7 ± 0.1 kcal/mol value listed in Table 1. The five sets of energetics in the literature can be placed in two groups. As discussed in section 1, one group (MR-CISD and SA-MCSCF) was part of a study[27] of coupled electronic surfaces where the emphasis was on a balanced description of two PESs, resulting in a compromise in the accuracy for the ground state PES which is of relevance here.

Their dissociation energy is lower (and in the case of SA-MCSCF very much lower) than experiment. As mentioned in section 1, the second group has a natural progression: the energetics of quadratic configuration interaction with single, double, and perturbative triple [QCISD(T)] with a large basis set,[21] the energetics of coupled cluster with single, double, and perturbative triple [CCSD(T)] with a complete basis set (CBS) extrapolation,[31] and energetics of the HCTH147 density functional theory (DFT)-based semiempirical molecular orbital method[25] with specific reaction parameters trained to the CCSD(T)/CBS results. The most accurate calculation, CCSD-(T)/CBS, agrees very well with the measured dissociation energy. As discussed in section 1, the least expensive of these five methods is still too expensive to implement in an *ab initio* molecular dynamics calculation, leading to only a few trajectories followed for short times. None of these calculations determined the isomerization saddle point and consequent energetics.

In order to determine the isomerization barrier, a relatively high level complete basis set-quadratic Becke3 (CBS-QB3) was carried out for all of the species in Figure 1. As seen in Table 1 and Figure 1, the resulting isomerization barrier is 2.5 kcal/mol higher than the resulting dissociation barrier. This is about half the difference calculated by a pioneering but less accurate polarization configuration interaction (POL-CI) approach 30 years ago.[24] At the energies of the photodissociation experiments, isomerization and dissociation will be competing processes. The CBS-QB3 compares quite well with the experimental D_0. The CBS-QB3 along with the only other CBS calculation [CCSD(T)] have smaller barriers for addition of H to C_2H_4 than any of the other methods in Table 1 or Figure 1. Small barriers have been found to be consistent with the measured addition kinetics rate constants.[7] The CBS-QB3 molecular structure and frequencies of C_2H_5 at equilibrium, the dissociation saddle point, and the isomerization saddle point can be found in Tables 2, 3, and 4, respectively. CBS-QB3

Table 2. C_2H_5 Equilibrium Geometry and Harmonic Frequencies (cm^{-1}) Calculated by Selected Methods[a]

	CBS-QB3	M05-2X	AIREBO	AIREBO-SRP
		Geometry		
R_{CC}	1.487	1.485	1.517	1.517
R_{CH1}	1.103	1.098	1.090	1.090
R_{CH2}	1.094	1.090	1.090	1.090
R_{CH3}	1.083	1.079	1.089	1.089
ϕ_1	112.0	111.6	110.9	110.9
ϕ_2	111.9	111.7	110.6	110.6
ϕ_3	120.9	120.8	121.8	121.8
θ_2	108.1	108.3	107.6	107.6
θ_3	117.7	118.0	116.2	116.2
α_3	172.8	173.2	174.9	174.9
		Frequencies		
	108	112	127	114
	477	486	655	589
	813	820	688	619
	980	995	1086	976
	1063	1088	1399	1258
	1192	1206	1407	1265
	1401	1419	1521	1367
	1465	1488	1800	1618
	1483	1504	1891	1700
	1483	1507	1957	1760
	2943	3003	2828	2542
	3035	3089	2864	2575
	3078	3134	2923	2628
	3139	3192	2928	2632
	3239	3297	2959	2660

[a]The geometry uses the coordinate system of ref 21. The bond lengths are in Å, and the angles are in degrees.

calculated values for C_2H_5 at equilibrium are quite similar to the large basis set QCISD(T) results of ref 21 and other high level calculations.[23] Experimental values for geometries are not readily available and measured vibrational frequencies are incomplete and anharmonic, making comparisons difficult.

To find much faster approaches for calculating the PES that would enable following many trajectories for long periods of time, the energetics (both dissociation and isomerization) of one semiempirical molecular mechanics method and two semiempirical molecular orbital (SEMO) methods different from HCTH147 were investigated. The two new SEMO methods were parametric method number 6 (PM6)[32] and M05-2X/CBSB7 (see the Glossary for details of this functional).[33] Both have been trained to experimental data drawn from a variety of chemical species. PM6 produced the largest dissociation energy (~12 kcal/mol higher than experiment), the lowest isomerization barrier, and no saddle point for H addition to C_2H_4. It will not be discussed further. In contrast, as can be seen in Table 1 and Figure 1, M05-2X with a relatively

dx.doi.org/10.1021/jp3099889 | J. Phys. Chem. A XXXX, XXX, XXX−XXX

Table 3. C_2H_5 Dissociation Saddle Point Geometry (Distance in Å, Angles in deg) and Harmonic Frequencies (cm^{-1}) Calculated by Selected Methods[a]

	CBS-QB3	M05-2X	AIREBO	AIREBO-SRP
		Geometry		
R_{CC}	1.335	1.334	1.376	1.310
R_{CH1}	2.238	2.147	1.625	2.238
R_{CH2}	1.084	1.081	1.106	1.090
R_{CH3}	1.085	1.081	1.090	1.090
ϕ_1	104.8	103.8	107.0	104.9
ϕ_2	121.7	121.4	120.2	124.5
ϕ_3	121.7	121.4	123.5	124.5
θ_2	116.5	117.0	115.4	110.9
θ_3	116.7	117.2	112.9	110.9
α_3	179.0	178.9	179.2	166.6
		Frequencies		
	−308[b]	−534	−6702	−367
	241	291	708	27
	273	326	808	272
	833	846	873	653
	961	987	942	843
	975	1008	1339	902
	1052	1064	1399	1399
	1238	1258	1530	1410
	1364	1380	1530	1543
	1470	1491	1673	1556
	1655	1682	1743	1618
	3129	3180	2799	2566
	3141	3191	2847	2594
	3202	3260	2873	2642
	3230	3285	2948	2643

[a]The geometry uses the coordinate system of ref 21. The bond lengths are in Å, and the angles are in degrees. [b]See ref 39.

Table 4. C_2H_5 Isomerization Saddle Point Geometry (Distance in Å, Angles in deg) and Harmonic Frequencies (cm^{-1}) Calculated by Selected Methods[a]

	CBS-QB3	M05-2X	AIREBO	AIREBO-SRP
		Geometry		
R_{CC}	1.492	1.487	1.650	1.650
R_{CH1}	1.297	1.293	1.300	1.297
R_{CH2}	1.081	1.078	1.079	1.079
R_{CH3}	1.081	1.078	1.079	1.079
ϕ_1	54.9	54.9	50.6	50.5
ϕ_2	119.4	119.2	118.9	119.0
ϕ_3	119.4	119.2	118.9	119.0
θ_2	118.6	119.1	115.8	115.8
θ_3	118.7	119.1	115.8	115.8
α_3	196.0	195.5	155.6	155.8
		Frequencies		
	−1928	−2082		−1928
	549	553		319
	746	763		576
	749	764		726
	790	799		821
	1131	1160		897
	1190	1206		923
	1274	1287		1256
	1418	1436		1662
	1441	1467		1666
	2217	2248		2217
	3139	3201		2630
	3144	3205		2647
	3243	3308		2713
	3266	3329		2716

[a]The geometry uses the coordinate system of ref 21. The bond lengths are in Å, and the angles are in degrees.

inexpensive basis set produced dissociation energetics essentially identical to HCTH147 that was trained specifically to the C_2H_5 system (although both methods are a few kcal/mol too high relative to CBS-QB3). M05-2X produces an isomerization barrier within 0.5 kcal/mol of that for CBS-QB3. In Tables 2−4, the geometries and frequencies of M05-2X are contrasted with those of CBS-QB3. The M05-2X equilibrium geometry and frequencies are in good agreement with the CBS-QB3 results. In Tables 3 and 4, M05-2X remains in superior agreement to CBS-QB3 results. Consequently, of the SEMO methods, M05-2X is the method of choice. Unfortunately, while M05-2X is a reasonable representation of the PES, in practice, direct *ab initio* trajectory calculations with M05-2X proved too slow for the purposes of this study.

Since semiempirical molecular mechanics potentials are evaluated with no diagonalization procedure for eigenvalues (as is required in SEMO methods), such potentials are computationally inexpensive to evaluate and well suited to trajectory studies. For this reason, we have tested the adaptive intermolecular reactive empirical bond-order (AIREBO)[34,35] semiempirical molecular mechanics potential using the most recent code supplied by the developer S. J. Stuart.[36] For our application, our AIREBO code produces a potential energy of the form described in the original AIREBO reference but with an improved set of parameter values (and with extensions that do not apply to the C_2H_5 system). AIREBO is designed to be able to describe reactions and systems far from equilibrium. However, it has been calibrated for condensed media application. The C_2H_5 study constitutes the first application of AIREBO to a gas-phase molecular system. The AIREBO energetics are listed in Table 1 and displayed in Figure 1, while the AIREBO geometries and frequencies are listed in Tables 2, 3, and 4 for the equilibrium, dissociation saddle point, and isomerization saddle point.

While AIREBO is orders of magnitude faster to evaluate than *ab initio* or SEMO methods, it has technical problems and accuracy issues that make it inappropriate for direct application to reaction 1. The technical problems concern two different discontinuities in the gradients of the potential. The first discontinuity arises from a linear interpolation of terms in the potential from a precalculated table of their values over a grid of interatomic distances. As the interatomic distance at the evaluation point passes through a node in the grid of distances, one of the two grid nodes that bracket the evaluation distance abruptly changes, resulting in a discontinuity in slope. Direct calculation of terms in the potential without table look-up eliminates this problem. The second discontinuity is in the behavior of AIREBO switches at isomerization. AIREBO for our application constructs the potential V from two parts:

$$V(\mathbf{x}) = V_{REBO}(\mathbf{x}) + V_{LJ}(\mathbf{x}) \quad (3)$$

where $\mathbf{x}$ is the geometry at which the potential is being evaluated, V_{REBO} is a reactive empirical bond order term, and V_{LJ} is a Lennard-Jones term for corrections to V_{REBO} at larger distances. Incorporated into V_{LJ} is a complicated product of three switches. For symmetric positions of the core H_2CCH_2

dx.doi.org/10.1021/jp3099889 | J. Phys. Chem. A XXXX, XXX, XXX−XXX

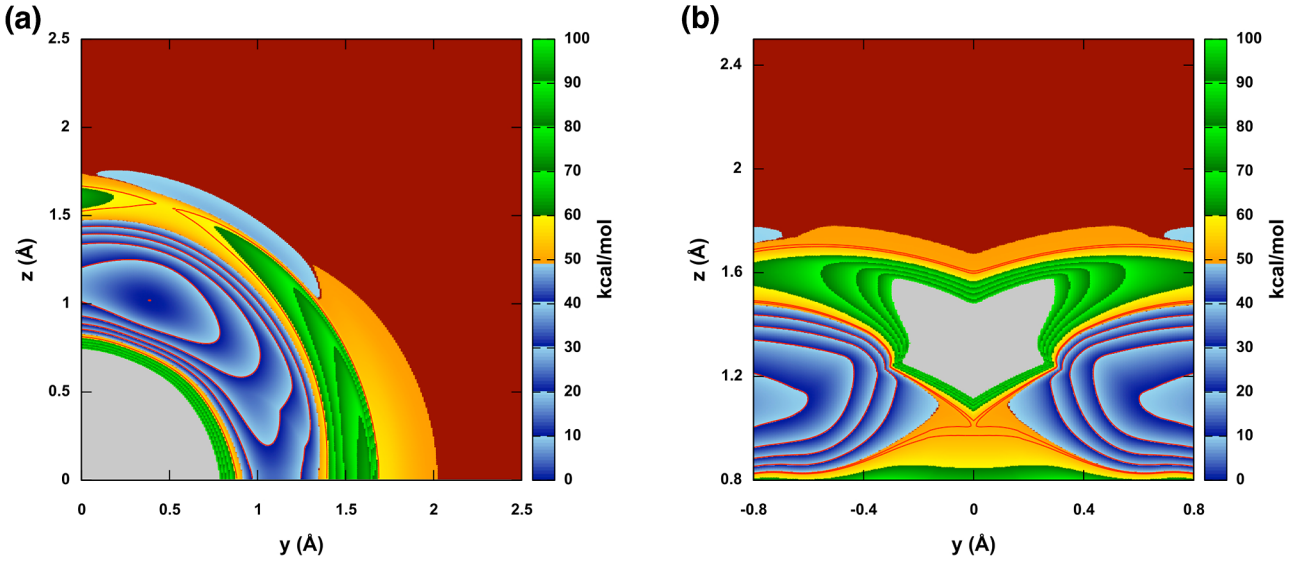

Figure 2. (a) The AIREBO-2010 potential energy as a function of (y,z) position of a H atom in the mirror symmetry plane with respect to the H_2CCH_2 fragment. The y axis is along the C−C bond with the origin on the right C atom. Blue designates energies lower than the H + C_2H_4 asymptote (in brick red). Yellow designates the first ∼10 kcal/mol above the asymptote. Green designates higher energies, while gray designates energies higher than 100 kcal/mol. The red contour at 58.1 kcal/mol indicates the dissociation saddle point. (b) The AIREBO-2010 potential energy as a function of (y,z) position of a H atom in the mirror symmetry plane with respect to the H_2CCH_2 fragment. The y axis is along the C−C bond with the origin on the midpoint of the C−C bond. Color coding as in part a except the two red contours at 50.8 and 52.0 kcal/mol indicate the isomerization saddle point.

during isomerization, this triple switch does not enforce a zero gradient for the isomerizing H atom's perpendicular passage through the C−C perpendicular bisector plane. The result is a gradient discontinuity in that C−C plane. How to remedy this problem requires discussion concerning accuracy issues.

AIREBO is insufficiently accurate for our purpose, as can be seen from Tables 1−4 and Figure 2. The two panels in Figure 2 represent a two-dimensional cut defined by the Cartesian position of one H atom through a 15 degree of freedom PES. The horizontal axis is coincident with the C−C bond. Both panels are for geometries constrained so that the plane defined by the C−C bond and the one H atom is a mirror symmetry plane for the remaining H_2CCH_2 structure. Six degrees of freedom orient two H atoms relative to the C−C bond in the H_2CCH_2 structure. If those two atoms are on the same side of the mirror symmetry plane, then the H_2CCH_2 structure is fully defined when the seventh degree of freedom, the C−C bond length, is specified. Each panel represents the lowest energy of the H atom with the H_2CCH_2 structure optimally relaxed. The two panels differ in the definition of the origin of the plot. For Figure 2a, the origin is one of the C atoms and incorporates the equilibrium and dissociation saddle point of C_2H_5. For Figure 2b, the origin is the midpoint of the C−C bond and incorporates the isomerization saddle point. While both panels display a continuous potential surface, the surface does have kinks in it (i.e., discontinuities in gradient). In Figure 2b, the kink along part of the isomerization dividing surface (i.e., $y = 0$ in the plot) is due to the second technical problem mentioned above. (The first technical problem concerning table look-up was corrected before making these plots.) However, there are other kinks, especially in Figure 2a, that are unconnected to the AIREBO PES but instead are due to the relaxation of the H_2CCH_2 structure in making the plot. There can be multiple minima in the seven degrees of freedom that define this structure, and which minimum is the lowest can abruptly change with the position of the H atom in the plot.

The results in Tables 1−4 and in Figure 2 indicate at least four significant inaccurate features with the native AIREBO PES:

- The energy of the C_2H_4 + H asymptote is ∼10 kcal/mol higher than experiment.
- The spatial extent of the bonded region of the PES is too condensed. The dissociation saddle point occurs at R_{CH1} distances that are ∼0.6 Å shorter than *ab initio* calculations.
- The dissociation barrier is ∼10 kcal/mol higher than the already too high C_2H_4 + H asymptote, while the isomerization barrier is comparable to the asymptote. This will result in a bias to isomerization inconsistent with the *ab initio* energetics for these two asymptotes.
- The isomerization region contains an unrealistically large repulsive region at R_{CH1} distances larger than the saddle point (the gray region in Figure 2b). Within this region, the peak repulsion exceeds 200 kcal/mol.

While these features are important, the scale of inaccurate features is ∼10 kcal/mol, while the energy scale of the photoexcitation experiments discussed above is ∼100 kcal/mol. Furthermore, the equilibrium properties compare reasonably well to *ab initio* calculations. The equilibrium geometry has as its maximum error an R_{CC} bond length that is 0.03 Å too long. The harmonic zero point energy is only ∼600 cm^{-1} too high or about 40 cm^{-1} per mode. The frequencies are consistently too high below 2000 cm^{-1} and consistently too low above 2000 cm^{-1}.

Taken together, the results above suggest that the general AIREBO model is a useful starting point for modifications specific to this PES that could reduce the major inaccuracies and address the discontinuity in forces discussed above. In the spirit of past work on other generic functional forms,[37,38] the modified PES will be call AIREBO-SRP for specific reaction parameters. AIREBO has tens of parameters, multiple switches

dx.doi.org/10.1021/jp3099889 | J. Phys. Chem. A XXXX, XXX, XXX−XXX

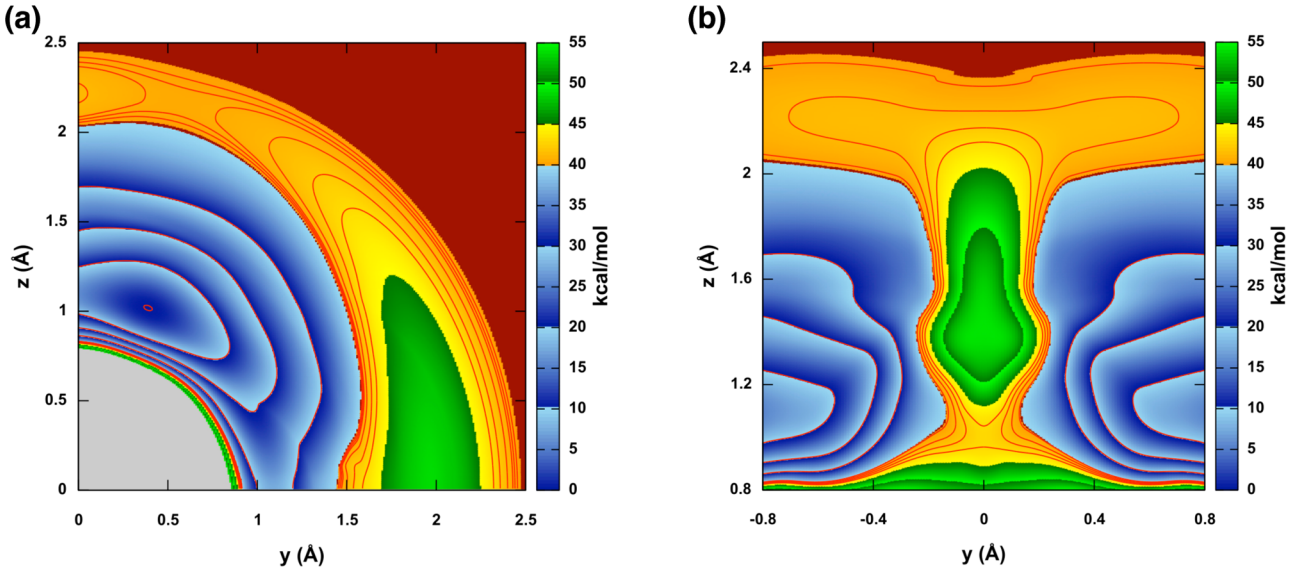

Figure 3. (a) The AIREBO-SRP potential energy as a function of (y,z) position of a H atom in the mirror symmetry plane with respect to the H_2CCH_2 fragment. The y axis is along the C−C bond with the origin on the right C atom. Blue designates energies lower than the H + C_2H_4 asymptote (in brick red). Yellow designates the first ∼5 kcal/mol above the asymptote. Green designates higher energies, while gray designates energies higher than 100 kcal/mol. Red contours at 40.0, 40.2, 40.4, 41.0, 42.0, and 43.0 kcal/mol indicate the dissociation saddle point. (b) The AIREBO-SRP potential energy as a function of (y,z) position of a H atom in the mirror symmetry plane with respect to the H_2CCH_2 fragment. The y axis is along the C−C bond with the origin on the midpoint of the C−C bond. Color coding as in Figure 3a except the red contours at 40, 41, 42, and 43 kcal/mol indicate the isomerization saddle point.

of a variety of forms, and pairwise functions whose form can be readily changed. Deep modifications are possible but would be sensible only in the context of systematic *ab initio* calculations to provide the basis for such changes. As the first use of AIREBO in the context of an isolated gas phase reaction, our goal will be more modestly directed at using only the *ab initio* information in Tables 1−4 and consequently only limited modifications will be explored.

There are three modifications that are easy to implement. First, the table lookup process is replaced by direct calculation, thus eliminating one source of the discontinuities in the forces. Second, the calculated potential energy as measured relative to the C_2H_5 equilibrium position can be scaled so as to recover the correct H + C_2H_4 experimental asymptote (see Table 1). The required scale factor is a fraction (0.808). (Unfortunately, it acts to reduce the equilibrium frequencies into poorer agreement with *ab initio* calculations.) Third, the Lennard-Jones terms in eq 3 can be eliminated. This has the double effect of eliminating the discontinuity in the forces with passage through the isomerization plane and drastically reducing the unphysical repulsive energies in the isomerization region, as seen in Figure 2b. In native AIREBO, the σ parameter in the Lennard-Jones potential for the C−H interaction is set to ∼2.8 Å. Although the switch for the Lennard-Jones potential is complicated, it can begin to turn on at C−H distances more than 1 Å less than σ, deep within the repulsive r^{-12} region of the potential. For this C_2H_5 application, the switch is not subtle enough to navigate through that repulsive region in a physically realistic way.

These three modifications result in a PES that is still too spatially constricted with dissociation and isomerization barriers still poorly related to *ab initio* calculations. To proceed further, the V_{REBO} in eq 3 must be more fully described:

$$V_{REBO}(x) = \sum_i \sum_{j\neq i} S\left(\frac{r_{ij} - r_{ij}^{min}}{r_{ij}^{max} - r_{ij}^{min}}\right)\left\{A_{ij}\left[1 + \frac{Q_{ij}}{r_{ij}}\right]e^{-\alpha_{ij}r_{ij}} - b_{ij}\sum_{n=1}^{3} B_{ij}^{(n)} e^{-\beta_{ij}^{(n)}r_{ij}}\right\} \quad (4)$$

where r_{ij} refers to interatomic distances that the vector **x** is composed of, S is a switch from 1 to 0 over a finite range determined by the min and max parameters in their arguments, b_{ij} are complicated functions of switches and parameters that determine the geometry-dependent bond order for the ij bond and include dependences on dihedral angles (and thus internal rotations), and everything else are AIREBO parameters. The spatial constriction of the native AIREBO PES is due to the fact that r_{CH}^{max} is set to 1.8 Å. Any H whose C−H distance exceeds that amount ceases to interact with any C atom; i.e., H has dissociated from the C_2H_4 fragment and is now in the H + C_2H_4 asymptotic region. Simply extending r_{CH}^{max} releases the spatial constriction at the price of much more inaccurate saddle point properties.

Consistent with a minimalist strategy, our additional modifications focus on only S for C−H interactions. All other parameters and switches remain the same. In particular, b_{ij} can include S for C−H interactions within its switches. For that application, S remains unchanged. Only as the outer switch in eq 4 and only for the C−H interaction will S be modified. Furthermore, r_{CH}^{min} = 1.3 Å will not be changed, meaning the equilibrium region of the PES will not be altered (other than by the scaling factor discussed above). Only the outer regions of S will be changed, and the changes will occur in two stages as discussed below. For both stages, the CBS-QB3 saddle point properties in Tables 3 and 4 will guide the modifications.

In the first stage, S is modified to represent the dissociation saddle point without regard for the implications for isomer-

dx.doi.org/10.1021/jp3099889 | J. Phys. Chem. A XXXX, XXX, XXX−XXX

ization. From Table 3, the saddle point location has R_{CH} = 2.2 Å. r_{CH}^{max} must be greater than 2.2 Å, and the final value selected is 2.5 Å. At that extended length, for $R_{CH} > r_{CH}^{min}$, there are extensive regions of the C−C−H angle $\phi \geq 90°$ where H interacts with both C's, including within the equilibrium region. This greatly complicates modifying S to reproduce CBS-QB3 saddle point properties while maintaining a physically reasonable PES for $\phi \geq 90°$. The solution to this difficulty is to make S a function of R_{CH} and ϕ. If ϕ_n is the angle for H bonded to the near carbon and ϕ_f is the angle for H bonded to the far carbon, then for $\phi_n \geq 90°$, it turns out that $\phi_f < 63°$ for $R_{CH} < 2.5$ Å. $S(R_{CH}, \phi \leq 60°)$ can then be set to the native AIREBO S with r_{CH}^{max} = 1.8 Å, ensuring that the equilibrium region is not perturbed. However, for $S(R_{CH}, \phi \geq 90°)$, r_{CH}^{max} is set to 2.5 Å and its native AIREBO functional form is abandoned in favor of a point by point fit over an (R_{CH}, ϕ) grid to a template analytic function designed to (1) reproduce the location, height, and two frequencies of the CBS-QB3 dissociation saddle point in (R_{CH}, ϕ) space, (2) be physically reasonable for $\phi \geq 90°$, and (3) join smoothly in value and slope the native AIREBO PES at $R_{CH} = r_{CH}^{min}$. Intermediate angular grid lines between $60° < \phi < 90°$ are filled out by a cubic switch in angle that match in value and angular slope the values at ϕ = 60 and 90° (note the angular slope at 60° is by construction 0.0). The final two-dimensional grid of S values for 1.3 Å $\leq R_{CH} \leq$ 2.5 Å and $60° \leq \phi \leq 180°$ is fit to a two-dimensional spline with the condition of zero slope on all four boundaries of the grid.

There are three technical details regarding this approach. First, the template potential is only 2 degrees of freedom with the presumption that the other 13 degrees of freedom are fully optimized. Consequently, iterative rounds of geometry relaxation are required to get the final values of S on the two-dimensional grid. Second, to converge saddle point properties, the grid must be considerably finer in the region of the saddle point than elsewhere. Hence, the final grid is regular but not uniform. Third, for C_2H_5, the two saddle points are in the mirror symmetry plane that lies along the C−C bond of the C_2H_4 fragment. This makes a ϕ dependence to S particularly useful. However, there is an azimuthal angle that can locate H out of the mirror plane. The absence of that dependence means that the out-of-plane saddle point frequency of either saddle point will only be accidentally represented in this approach.

Figure 3a and the AIREBO-SRP column in Tables 1−3 display the result of modifications to native AIREBO up to this stage. Table 1 shows a correct experimental asymptote and a correct[39] CBS-QB3 energy relative to that asymptote. As a consequence of a transcription error in the CBS-QB3 dissociation barrier height, the matched value for the AIREBO-SRP PES is 40.3 kcal/mol rather than 40.5 kcal/mol, as now listed in Table 1. Table 2 shows that the equilibrium location is unchanged from that of native AIREBO, but the frequencies are all reduced because of the scale factor. Despite this reduction, in general, the frequencies are still too high at the low end and too low at the high end relative to CBS-QB3 values. Table 3 shows that the CBS-QB3 saddle point values for R_{CH1} and ϕ_1 values are exactly reproduced and the other geometric parameters are not far off. The imaginary frequency and the in-mirror-plane frequency of the dissociating H are also in agreement[39] with CBS-QB3. Similarly to Table 1, as a consequence of a transcription error in the CBS-QB3 tunneling frequency, the matched value for the AIREBO-SRP PES is −367 cm^{-1} rather than −308 cm^{-1}, as now listed in Table 3. The out-of-mirror-plane frequency, while smaller than the in-mirror-plane frequency in agreement with CBS-QB3, is an order of magnitude too small relative to the CBS-QB3 value. This is a consequence of the absence of an azimuthal angular dependence in the modified switch. The remaining frequencies are too high at the low end and too low at the high end, as in Table 2 for the equilibrium frequencies.

The last stage of modifications concerns the isomerization region. The angle the isomerizing H atom makes with either end of the C−C axis is acute. The modification strategy above is inapplicable to this region because the switch must be simultaneously modified for two C−H interactions. The last stage of modifications takes advantage of the fact that the isomerization saddle point is located at the intersection of two symmetry planes, namely, the mirror symmetry plane and the C−C perpendicular bisector plane. Along the line of intersection, the two C−H interactions are identical. Following the process used in the dissociation region, the switch value needed to reproduce a template potential along that line for a fully relaxed C_2H_4 fragment can be determined. The template potential can be shaped to have the CBS-QB3 saddle point properties along that line, to merge seamlessly into the native AIREBO PES at values of R_{CH} that are interior to the saddle point, and to be physically reasonable at distances much larger than the saddle point. If the resulting switch value is call S_{iso}, then S must transform into S_{iso} as $|R_{C1H} - R_{C2H}|$ approaches zero (where C1 and C2 indicate the two carbons). This is accomplished with a new switch S' operating on the argument $q = |R_{C1H} - R_{C2H}|/\Delta R$, where ΔR is the range over which S' applies. If S_{mod1} is the modified switch after the first stage of modifications discussed previously and if S_{mod2} is the final switch after this second stage of modifications, then

$$S_{mod2} = S'(q)S_{iso} + [1 - S'(q)]S_{mod1} \quad (5)$$

for the C1−H and C2−H interactions. Equation 5 requires that $S'(q \geq 1) = 0$ and $S'(0) = 1$, while continuity in value and derivative require that the derivative $S'(q) = 0$ for q = 0 or 1. This can be accomplished by an even powered fourth order polynomial in q. However, in this scheme, $S'(q)$ determines the imaginary frequency at the saddle point. $S'(q)$ was given more flexibility to set this frequency by making it a sixth order polynomial of the form:

$$S'(q) = 1 - 6q^2 + 9q^4 - 4q^6 + 4wq^2(1 - q^2)^2 \quad (6)$$

where w is a parameter that alters the width of the switch. If $0.75 \leq w \leq 1.5$, $S'(q)$ has no extraneous extrema.

Figure 3b and the AIREBO-SRP column in Tables 1 and 4 display the result of modifications to native AIREBO that include isomerization. For these results, ΔR = 0.196 and w = 0.95, parameter values that leave unchanged the first stage modifications displayed in Figure 3a and Tables 1−3. Table 1 shows a correct CBS-QB3 isomerization saddle point energy relative to the experimental H + C_2H_4 asymptote. Table 4 shows that the CBS-QB3 saddle point value for R_{CH1} is exactly reproduced. The perpendicular distance of the saddle point from the C−C midpoint (i.e., z in Figure 3b) is also exactly reproduced but not displayed in the table. Reproducing those two distances results in a ϕ_1 value that is somewhat too low, unlike the exact reproduction of the CBS-QB3 value in Table 3 for dissociation. While ϕ_1 is too low, R_{CC} is too large but all the other distances and angles are as approximately correct in Table

dx.doi.org/10.1021/jp3099889 | J. Phys. Chem. A XXXX, XXX, XXX−XXX

4 for isomerization as they are in Table 3 for dissociation. The large imaginary frequency and the large C−H stretch frequency along the perpendicular direction (z in Figure 3b) are in exact agreement with CBS-QB3. Unlike the results in Table 3 for dissociation, the out-of-mirror-plane frequency for the isomerizing H at 1256 cm^{-1} is quite close to the CBS-QB3 value of 1274 cm^{-1}. Like the Table 3 results, the remaining highest frequencies are too low. Unlike the Table 3 results, the lower frequencies (<2000 cm^{-1}) are a mix of too high and too low.

Overall, the AIREBO-SRP developed here avoids discontinuities in the gradients, displays CBS-QB3/experimental energetics for dissociation/isomerization processes, has the correct general spatial extent, and approximates the CBS-QB3 geometries and frequencies of the equilibrium and two saddle points. For these three structures, the root-mean-square (rms) error on distances relative to CBS-QB3 values varies from ∼0.015 Å for equilibrium and the dissociation saddle point to 0.08 Å for the isomerization saddle point (due to the 0.16 Å discrepancy for R_{CC}). The rms error in the angles varies from ∼2.5 to ∼6.5°. The rms error in frequencies is more substantial, ranging from ∼300 to ∼350 cm^{-1}. These errors tend to be in the same direction so that the difference from CBS-QB3 for the change in zero point energy between saddle point and the equilibrium geometry is ∼90 cm^{-1} for dissociation and ∼550 cm^{-1} for isomerization out of an average zero point energy of ∼11 000 cm^{-1}. The AIREBO-SRP PES will be used for the trajectory runs whose results will be described in the rest of this article. As a measure of continuity of the AIREBO-SRP gradients, no propagation errors are encountered for traditional step sizes (∼0.05 fs) and energy conservation errors ≥0.7% of the total energy are restricted to <1% of the trajectories run. On the native AIREBO surface, energy conservation errors of ≥1% of the total energy occurred for ∼60% of the trajectories.

2.2. Initial Conditions and End of Propagation Conditions. The trajectories were calculated using a version of GENDYN[40] interfaced with AIREBO-SRP. Microcanonical ensembles of 10 000 trajectories were calculated for total energies at 10 kcal/mol intervals over the range 100−150 kcal/mol. The initial conditions were prepared by starting with the ethyl radical at the AIREBO-SRP equilibrium geometry (see the last column in Table 2). A Markov walk[41] of 2 million steps was carried out to move the system away from equilibrium to a random phase space point. Since the radical is symmetric, the Markov walk was restricted on only one of the double wells by placing a reflecting barrier at the saddle point for the migration of a H atom from the methyl carbon to methylene carbon. At each Markov step, all of the Cartesian coordinates were changed by a random fraction of 0.11 Å with sampling over the range of 2.0 Å for each coordinate; these parameters gave acceptance/rejection ratios over the range 0.44−0.64. The configuration at the end of the initial randomization walk was used to generate the initial conditions of the first trajectory, and the initial conditions for subsequent trajectories were obtained by performing 10 000 Markov steps from the configuration used to generate the initial conditions of the previous trajectory. The initial conditions were set so that the total angular momentum was zero.

The trajectories were integrated using velocity Verlet with a time step of 0.05 fs, which gave an integration accuracy that resulted in less than 1% of the trajectories having greater than 1 kcal/mol drift for the total energy of 150 kcal/mol. The forces were obtained by central differencing with the distance increment 1.0×10^{-5} Å.[42] A trajectory was ended if a C−H bond length exceeded 2.5 Å (that is, dissociation occurred) or the total integration time exceeded 100 ps. Isomerization was defined to have occurred when a hydrogen atom crossed the isomerization plane and the resulting new C−H bond underwent at least one inner and one outer turning point (i.e., at least one vibration) without recrossing the isomerization plane. The time of the isomerization was taken to be the time at which the barrier was crossed.

3. TRAJECTORY RESULTS AND DISCUSSION

As described above, 10 000 trajectories were followed for 100 ps at six different energies that span the energies of the photodissociation experiments. The results of these simulations are organized below under the topics of dissociation/isomerization dynamics, product translational energy distributions, and isotopic scrambling.

3.1. Dynamics of Dissociation and Isomerization. In order to study both dissociation and isomerization, the trajectories can be represented in terms of the time-dependent normalized population $P_i(t)$ of trajectories that at time t have undergone only i isomerizations and have not yet dissociated. Initially, no trajectories have undergone isomerization so $P_0(t)$ can only decay with time by isomerization or dissociation. All other $P_i(t)$ will initially grow with time from isomerization of $P_{i-1}(t)$ and decay at later times from dissociation or isomerization. The solid lines of Figure 4 show the normalized populations of the C_2H_5 isomers that have had 0 to 3 isomerizations, for the energies of 100, 130, and 150 kcal/mol. (The figure also shows with dash−dot lines kinetic model fits to these populations that will be discussed in the next section.) The results at all three energies are relatively similar with primarily only the time scale changing. These results show two important features of the dynamics. First, isomerization populations are on the order of 20% of the initial population and multiple isomerizations are clearly evident. At thermal energies (at least 60 kcal/mol lower than any of these results), isomerization will poorly compete with dissociation because, as shown in Figure 1 and Table 1, the isomerization barrier is 2.5 kcal/mol higher than dissociation.

The second feature of these results is the absence of very long-lived trajectories. Even at the lowest energy represented here, all the trajectories were followed until they dissociated. All of the trajectories dissociated within 100 ps integration time. These results do not support any significant amount of C_2H_5 dissociating with a rate of 10 ns. However, this does not mean that the isomer populations dissociate with a single exponential decay. In Figure 5, the $P_0(t^*)$ trajectory results are plotted versus an energy-scaled time t^* along with optimal single exponential fits. t^* is $t/(1 + [0.1(150 - E)]^{1.75})$ and is solely designed to allow $P_0(t)$ for E = 100 and 130 kcal/mol to be plotted with sufficient resolution on the same graph as $P_0(t)$ for E = 150 kcal/mol. The single exponential fit is for a unit prefactor (to preserve a *normalized* population in the fit) and is optimized to minimize the absolute rms error. As the figure shows, at low energies, a single exponential fit is a good representation. However, at the higher energies, at both high and low values of P_0, there are noticeable deviations on a maximum scale approaching 0.05.

The decay of $P_0(t)$ is due to both isomerization and dissociation. Tests at E = 150 kcal/mol show that both the dissociation products and the isomerization products from $P_0(t)$ decay have a comparable deviation from a single exponential model. Although Figure 5 displays behavior for

dx.doi.org/10.1021/jp3099889 | J. Phys. Chem. A XXXX, XXX, XXX−XXX

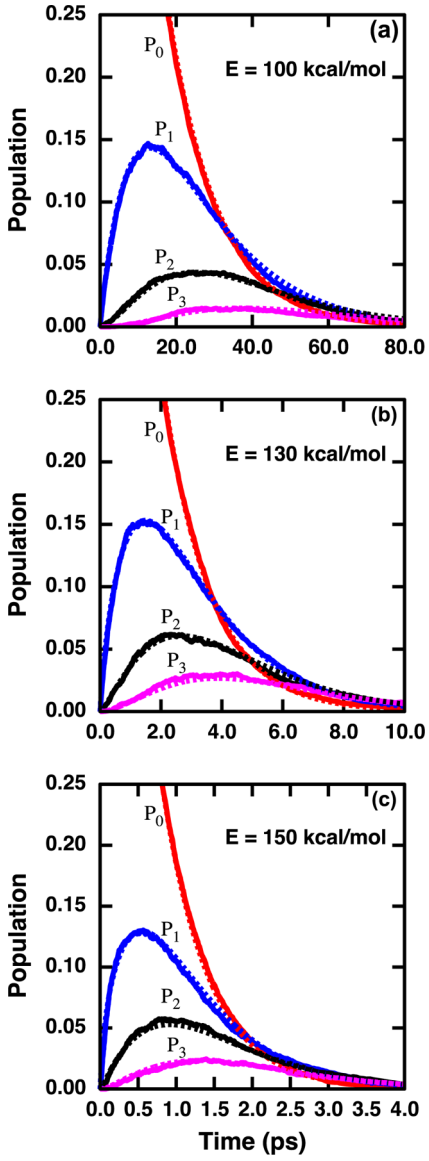

Figure 4. Normalized trajectory populations $P_i(t)$ (solid lines) and corresponding kinetics model fits for i = 0, 1, 2, and 3 for a total energy E of 100 kcal/mol (panel a), 130 kcal/mol (panel b), and 150 kcal/mol (panel c). See text for details.

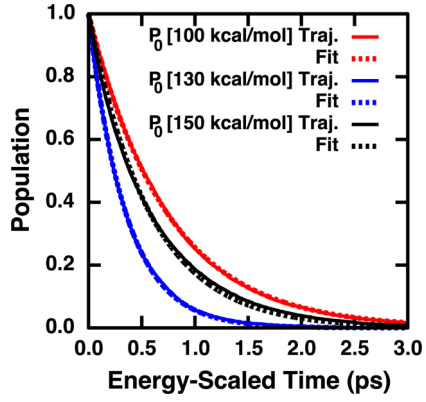

Figure 5. $P_0(t^*)$ versus energy-scaled time t^* for E = 100, 130, and 150 kcal/mol. See text for details.

only P_0, the overall H product formation rate (which is what experiments directly measure) also shows multiexponential behavior at high energies but single exponential behavior at low energies. However, the multiexponential behavior observed does not involve multiple rate constants that differ by many orders of magnitude, as suggested by the Chen[8] and Fischer[11] groups.

All the trajectories used in this study have no initial rotational energy. As such, no meaningful differential scattering cross section can be calculated. However, as seen in Figure 4, at all energies studied, the C_2H_5 lifetime exceeds 1 ps. The rotational period of C_2H_5 is ~1 ps or less, depending on the degree of rotational excitation. Thus, the expectation is that the angular scattering would be nearly isotropic, in agreement with experimental measurements.

3.2. Translational Energy Distributions. Figure 6 shows the product translational energy distribution and the corresponding optimal Maxwell distribution fit for the highest and lowest energies studied. $\langle f_T \rangle$, the fraction of product energy released into translation, is listed for each energy in Table 5 along with the temperature derived from the Maxwell distribution fit. As the energy increases, the trajectory and Maxwell distributions shift to higher and broader peaks. However, the Maxwell–Boltzmann distribution is not peaked enough to well represent trajectory results. From Table 5, $\langle f_T \rangle$ varies by ~0.02 from 0.14 at 100 kcal/mol to 0.12 at 150 kcal/mol. Hase et al.[19] calculated a value of 0.18 at 100 kcal/mol on a different PES. The most recent and probably most reliable experimental measurement[11] is 0.19. As discussed earlier, the product translational energy distribution is bimodal, of which only the lower energy component is relevant to unimolecular decay on the ground state PES. Consequently, the experimental value can be complicated by the decomposition. However, it is

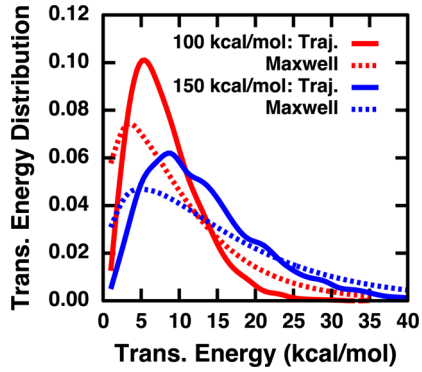

Figure 6. Product translational energy distributions from trajectories and from the corresponding least-squares fit Maxwell distribution.

Table 5. $\langle f_T \rangle$ Calculated by Trajectories and T_{MAX} from the Maxwell Distribution Fit to the Product Translational Energy Distribution

E (kcal/mol)	$\langle f_T \rangle$	T_{MAX} (K)
100	0.139	3300
110	0.133	3700
120	0.129	4100
130	0.126	4500
140	0.123	4900
150	0.121	5200

dx.doi.org/10.1021/jp3099889 | J. Phys. Chem. A XXXX, XXX, XXX–XXX

most likely the case that the AIREBO-SRP PES results in a somewhat low value for $\langle f_T \rangle$.

3.3. Isotopic Scrambling. For both ends of our energy range, trajectory studies analogous to Figure 4a and c were carried out for CD_2CH_3. The fraction F_H of products that constitutes H + CD_2CH_2 was determined and is reported in Figure 7 as the red symbols; it is substantially less than unity,

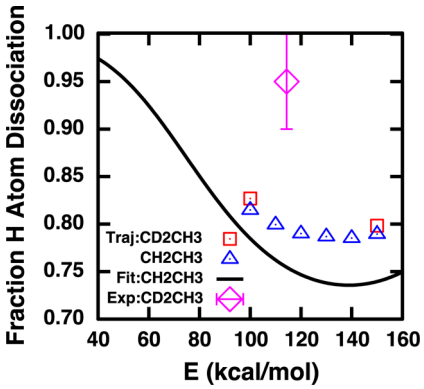

Figure 7. The fraction of dissociations of CD_2CH_3 that produce H atoms as a function of energy. Trajectory calculations for CD_2CH_3 (red symbols), trajectory calculations for CH_2CH_3 with interpolated results from CD_2CH_3 (blue symbols), and kinetics model fits to CH_2CH_3 with statistical isotopic fractions (black line). See text for details.

about 0.8. In contrast and as shown in the figure, the most recently measured[11] F_H in this energy range is greater than 0.9. This PES appears to allow too much isotopic scrambling from isomerization. Figure 8 examines F_H for each isomer population

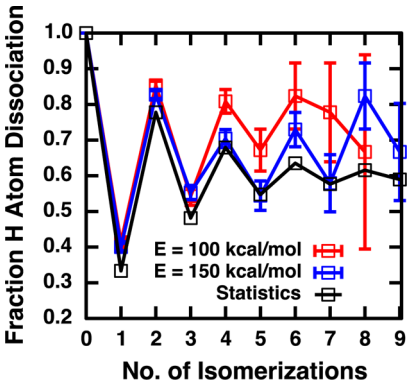

Figure 8. As a function of the number of isomerizations, the fraction of dissociations of CD_2CH_3 that produce H atoms from a statistical model and from trajectories at E = 100 and 150 kcal/mol. Error bars on trajectory results represent one σ. See text for details.

for the low (red line) and high (blue line) energy. For early isomer populations, the high and low energy results alternate in synchronization between high and low H fractions. For the later isomer populations, the sampling statistics, represented by one σ error bars, become too poor to distinguish the two distributions. Intermediate isomer populations do seem to favor more H dissociation at lower energies.

The alternation in Figure 8 can be easily understood from a statistical model in which H and D can equally well isomerize or dissociate from the methyl end of the radical. With such an assumption, CD_2CH_3 can only dissociate to H atoms giving an F_H of 1. However, CD_2CH_3 can isomerize to produce CH_2CHD_2 whose F_H is 1/3. CH_2CHD_2 can isomerize to produce 67% of the time CH_2DCHD (F_H of 2/3) and 33% of the time CH_3CD_2 (F_H of 1). This results in an F_H of 7/9. The generalization of this process produces an F_H of the ith isomer, $F_H(i)$, of

$$F_H(i) = 0.6 + 0.4(-2/3)^i \quad (7)$$

which is the black line in Figure 8. Dissociation after a very large number of isomerizations gives an $F_H(i \gg 1) = 0.6$ or the ratio of H atoms to all hydrogenic atoms in CD_2CH_3, the expected result for complete isotopic scrambling.

The trajectory results always show a $F_H(i)$ higher or at best the same as the statistical result of eq 7, implying that H and D do *not* behave equally with regard to isomerization and dissociation. H atoms are consistently more prone to dissociation than D atoms, and that propensity might increase as the energy decreases. While that is the conclusion to draw from Figure 8, this conclusion may be sensitive to the definition of isomerization. As discussed earlier, isomerization here occurs when the isomerizing atom crosses the isomerization plane and undergoes an outer and an inner turning point. By this definition, a H atom that crosses the isomerization plane and then directly (i.e., no outer turning point) dissociates without ever recrossing the isomerization plane would be said to dissociate without isomerizing. At E = 150 kcal/mol, the C_2H_5 trajectories of Figure 4c were rerun with termination upon either dissociation or upon an isomerization defined *solely* by crossing the isomerization plane. Comparison with the original trajectory run indicates that ~20% of the original P_0 dissociations crossed the isomerization plane at least once. If a substantial number of those trajectories crossed the plane only once on the way to directly dissociate with no further turning points, then an isomerization definition based solely on crossing the isomerization plane would result in the hydrogenic atom that just isomerized having a greater propensity to dissociate than the two other hydrogenic atoms already resident on that side of the radical. This would violate the statistical assumption underlying eq 7 and perhaps quantitatively change the degree of alternation seen in the trajectory results in Figure 8.

Applying the alternations in Figure 8 to the asymptotic product population for each isomer from the isotopically pure CH_2CH_3 trajectory runs are shown as the blue triangles in Figure 7. In this application, the calculated alternations at E = 100 and 150 kcal/mol are connected by a linear interpolation in energy. At the two end point energies where no interpolation error is involved, the conversion of CH_2CH_3 results in F_H for the mixed isotope CD_2CH_3 having less than a 0.02 error. As seen previously in Table 1, the best available electronic structure calculations have an isomerization barrier 2.5 kcal/mol higher than the dissociation barrier. This implies that, as E approaches the C−H dissociation energy of ~40 kcal/mol, trajectory calculations of F_H will approach unity. In this context, the blue-triangle trajectory results in Figure 7 display a high-energy minimum or at least a plateau in the energy dependence of F_H. The minimum value of ~0.8 is midway between the possible extremes of 1.0 (dissociation dominates isomerization) and 0.6 (isomerization dominates dissociation).

As discussed earlier, the AIREBO-SRP PES was only calibrated to a variety of calculated isomerization and dissociation saddle point properties. The total energy involved in the measured F_H value in Figure 6 is more than twice the C−

dx.doi.org/10.1021/jp3099889 | J. Phys. Chem. A XXXX, XXX, XXX−XXX

H dissociation energy and therefore samples regions of the PES far removed from saddle points. The comparison to experiment in Figure 7 indicates that the region of the isomerization plane on the AIREBO-SRP PES is too "open", allowing too much isomerization that suppresses F_H substantially below the measured value.

4. KINETICS ANALYSIS OF TRAJECTORIES

The representation of the trajectory results in terms of populations (as in Figure 4) calls to mind coupled kinetics models, in which species that react with each other are modeled by first order kinetics equations. The solutions of the first order kinetics equations give the species concentrations as a function of time that parametrically depend on the reaction rates. The populations displayed in Figure 4 have the property of a cascade in which there is no process that transforms a population $P_i(t)$ into a "prior" population $P_{j<i}(t)$. The kinetics of cascades can often be represented analytically, leading to representations of $P_i(t)$ that can be least-squares fit to the trajectory results to produce optimal values of the rate parameters in the kinetics model. This section describes such a kinetics model. In addition to their interpretive value, validated kinetics models can be extrapolated to higher or lower energies and to longer times to gain a more comprehensive understanding of the processes studied by the trajectories.

A successful kinetics model must be able to describe dissociation and isomerization processes for a cascade of isomers, i.e., Figure 4. For quantitative accuracy, it must be able to describe the emergence of multiexponential decay with increasing E, i.e., Figure 5. For extrapolation as a function of energy, each optimized parameter value at the six different values of E where trajectories were calculated must have a "smooth" energy dependence. Several kinetics models were investigated of which the simplest one to satisfy the three conditions is as follows. At each energy, phase space is divided into two regions whose volumes are proportional to a parameter F_1 and $F_2 = 1 - F_1$. Trajectories in region 1 over time hop into region 2 with a rate k_{12}. Trajectories hop from region 2 to region 1 with a rate k_{21} that in general is not equal to k_{12}. Isomerization and dissociation *only* occur out of region 2 with rates k_{DIS} and k_{ISO}. If $C_i(t)$ is the population in region 2 of the ith isomer and $Q_i(t)$ the corresponding population in region 1, then from the description above the first order kinetics equations are

$$\begin{aligned} dC_i(t)/dt &= -(k_{DIS} + k_{ISO} + k_{21})C_i(t) + k_{ISO}C_{i-1}(t) \\ &\quad + k_{12}Q_i(t) \\ dQ_i(t)/dt &= -k_{12}Q_i(t) + k_{21}C_i(t) \end{aligned} \tag{8}$$

where $C_{i<0}(t) = Q_{i<0}(t) = 0$, $C_0(0) = F_2$, and $Q_0(0) = F_1$.

Since $P_i(t) = C_i(t) + Q_i(t)$, it is easy and more convenient to convert the above into equations in those for $C_i(t)$ and $P_i(t)$:

$$\begin{aligned} dC_i(t)/dt &= -(k_{DIS} + k_{ISO} + k_{21} + k_{12})C_i(t) \\ &\quad + k_{ISO}C_{i-1}(t) + k_{12}P_i(t) \\ dP_i(t)/dt &= -(k_{DIS} + k_{ISO})C_i(t) + k_{ISO}C_{i-1}(t) \end{aligned} \tag{9}$$

where $C_{i<0}(t) = P_{i<0}(t) = 0$, $C_0(0) = F_2$, and $P_0(0) = 1$.

The above equations can be analytically solved as

$$\begin{aligned} P_i(t) &= e^{-at}\sum_{j=0}^{i} A_{i,j}t^j + e^{-bt}\sum_{j=0}^{i} B_{i,j}t^j \\ C_i(t) &= e^{-at}\sum_{j=0}^{i} C_{i,j}t^j + e^{-bt}\sum_{j=0}^{i} D_{i,j}t^j \end{aligned} \tag{10}$$

where

$$\begin{aligned} a &= \frac{S + \sqrt{S^2 - 4[k_{DIS} + k_{ISO}]k_{12}}}{2} \\ b &= \frac{S - \sqrt{S^2 - 4[k_{DIS} + k_{ISO}]k_{12}}}{2} \end{aligned} \tag{11}$$

where $S = k_{DIS} + k_{ISO} + k_{12} + k_{21}$.

The four sets of expansion coefficients are best expressed by recursion expressions. The following expressions are the initial values for the recursion:

$$\begin{aligned} A_{00} &= -\frac{b - F_2[k_{DIS} + k_{ISO}]}{a - b} \\ B_{00} &= \frac{a - F_2[k_{DIS} + k_{ISO}]}{a - b} \\ C_{00} &= \frac{aA_{00}}{k_{DIS} + k_{ISO}} \\ D_{00} &= \frac{bB_{00}}{k_{DIS} + k_{ISO}} \end{aligned} \tag{12}$$

For $i > 0$, the recursions for A_{ij} take the form

$$\begin{aligned} A_{i,j>0} &= \\ &\quad -\frac{k_{ISO}[b - k_{DIS} - k_{ISO}]C_{i-1,j-1} + k_{ISO}jC_{i-1,j+1} - j(j+1)A_{i,j+1}}{j(a-b)} \\ A_{i>1,0} &= \frac{A_{i1}}{a - b} \\ A_{1,0} &= \frac{A_{11} - k_{ISO}F_2}{a - b} \end{aligned} \tag{13}$$

In eq 13, $A_{k,l>k} = C_{k,l>k} = A_{kl<0} = 0$. The recursion for B_{ij} is the same form as eq 13 with the substitution of (b, a) for (a, b), D_{kl} for C_{kl}, and B_{kl} for A_{kl}. For $i > 0$, the recursion for C_{ij} is

$$C_{ij} = \frac{aA_{ij} - (j+1)A_{i,j+1} + C_{i-1,j}}{k_{DIS} + k_{ISO}} \tag{14}$$

where $A_{k,l>k} = C_{k,l>k} = 0$. The recursion for D_{ij} is the same form as eq 14 with the substitution of a for b, D_{kl} for C_{kl}, and B_{kl} for A_{kl}.

This kinetics model has the isomerization and dissociation processes explicitly represented through specific rate constants. The form of the analytic solution has all isomer populations controlled by two exponential terms whose relative weights and differences in arguments are controlled by adjustable parameters. The model heuristically represents the common explanation for multiexponential unimolecular dissociation, namely, that IVR is too slow to keep phase space uniformly occupied during fast bond-breaking processes, leading to a breakdown in the statistical model responsible for single exponential decay. In the above kinetics model, the complex IVR process has been drastically simplified to the coupling of

dx.doi.org/10.1021/jp3099889 | J. Phys. Chem. A XXXX, XXX, XXX−XXX

two regions of phase space. Strong coupling allows all of the phase space to readily participate in dissociation or isomerization. Weak coupling means that the F_1 volume of phase space lags in its participation that in turn affects the rate of dissociation and isomerization.

The kinetics model just described has five adjustable parameters, k_{DIS}, k_{ISO}, k_{12}, k_{21}, and F_1. This model does represent the trajectory data quite well, but a simpler model fits the data almost as well. The simplicity is achieved by relating k_{12} and k_{21} to F_1. k_{12} and k_{21} can be thought of as backward and forward rates that control the approach to equilibrium between the two divided regions of phase space. Their ratio can be thought of as an equilibrium constant, and such constants are always ratios of the phase space volume of the two species that are in equilibrium. To the degree that the phase space volume of regions 1 and 2 is proportional to F_1 and $1 - F_1$, then

$$k_{21} = \frac{F_1}{1 - F_1} k_{12} \tag{15}$$

This relationship reduces the number of adjustable parameters to four and is the version of the kinetics model used to fit the trajectory results at all six energies.

The four parameters in the kinetics model were fit by nonlinear least-squares techniques to the trajectory values for $P_i(t)$ for i = 0, 1, 2, 3. For each value of energy, there are a little more than 2000 values of t for which $P_i(t)$ was recorded for each value of i. The resulting ~8000 data points were treated equally in the least-squares process to arrive at optimal parameters that minimized the rms error. Initial runs showed that the optimal value of F_1 varied significantly from energy to energy, producing optimal values in the other parameters that had an irregular dependence on energy. However, near optimal values of F_1 insignificantly raised the rms error. Imposing on F_1 various low order polynomial dependencies in E indicated that a constant F_1 with respect to E was both the simplest and optimal representation. The final least-squares solution optimized k_{DIS}, k_{ISO}, and k_{12} independently at each energy to minimize the rms error at that energy but optimized a constant value of F_1 to minimize the six term sum of the rms errors at each energy.

In Figure 4, the dash−dot lines represent the resulting optimal fit for three of the six energies. The other three energies are quite comparable. The rms errors range from 0.0014 (E = 120 kcal/mol) to 0.0028 (E = 150 kcal/mol). Since the populations are all normalized, this scale of rms errors indicated overall fits at the few tenths of a percent level. Figure 4 indicates that the emergence of multiexponential decay at the higher energies in $P_0(t)$ is captured well by this model. Although the kinetics model results are not plotted in Figure 5 that highlights the emergence of multiexponential behavior, they would be nearly indistinguishable from the trajectory results. The energy dependence of the optimal values of k_{DIS}, k_{ISO}, and k_{12} is displayed by the symbols in Figure 9; the optimal value of F_1 is 0.71. The energy behavior of all three parameters is reasonably smooth and regular. The solid lines in Figure 9 are a least-squares fit of the natural log of the parameters to a quadratic in the energy. k_{DIS} and k_{ISO} are exceptionally well represented, but there are some relative minor deviations in the fit of k_{12}.

The results in Figure 9 confirm the expected behavior. At low energies, $k_{12} \gg k_{DIS} + k_{ISO}$ and a single exponential dominates the decay. Analysis of eq 11 shows that the exponential

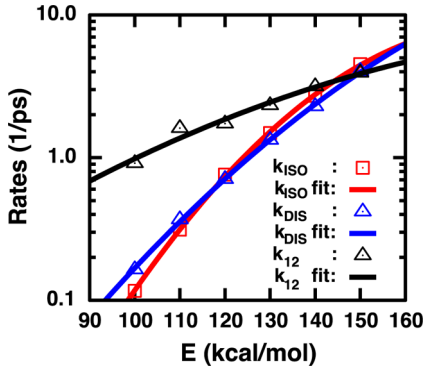

Figure 9. Least-squares values of the three rate constants in the kinetics model versus energy (symbols). Least-squares fits of the energy dependence of the optimal values of the three rate constants (solid lines).

arguments a and b are proportional to k_{12} and $k_{DIS} + k_{ISO}$, respectively, but according to eq 13, the faster decay receives very little amplitude and is just a short-time transient. At high energies, k_{12}, k_{DIS}, and k_{ISO} are all comparable and a biexponential decay emerges. From the trends in Figure 9, at higher energies, still $k_{12} \ll k_{DIS} + k_{ISO}$. Then, a and b will retain the same proportionality to the rates but the amplitudes of those terms will be proportional to F_2 and F_1, respectively. For the optimal F_1 value of 0.71, biexponential unimolecular decay would be quite evident. However, nothing in this analysis of our trajectory results points to an extremely slow rate. Rather, all rates increase with E but not equally fast. The slow rates measured by the Chen and Fischer groups would require rates orders of magnitude lower than those in Figure 9.

The results in Figure 9 indicate that k_{DIS} and k_{ISO} are comparable throughout the energy range of the trajectories. Considering that the barriers to dissociation and isomerization are quite close to one another (relative to values of E more than twice either barrier), this is perhaps not a surprising result. When examined more quantitatively, the small differences between k_{DIS} and k_{ISO} do have consequences. As seen in Figure 9, there is a finite energy range over which $k_{ISO} > k_{DIS}$. As discussed earlier, the more isomerization dominates dissociation, the lower F_H becomes. Because the relative size of k_{ISO} to k_{DIS} is not monotonic in energy, F_H will also not be monotonic in energy. This is illustrated by the black line in Figure 7 where F_H is calculated over an extended energy range using the energy dependence of the fit in Figure 9 and the statistical alternation in Figure 8. The minimum in F_H corresponds to the maximum in k_{ISO} relative to k_{DIS} in Figure 9. The blue triangles in Figure 7 involve only an interpolation of trajectory-calculated alternations in Figure 8. They also display a shallow minimum, indicating that the fit is representing a real feature of the trajectory results. This suggests that precise measurements of the energy dependence of isotopic scrambling could reveal subtle variations in the competition between isomerization and dissociation.

The energy dependence of the rates as displayed in Figure 9 has a limited range of validity when extrapolated beyond the energy range of the trajectory calculations. At the low energy end, the higher barrier to isomerization relative to dissociation means that isomerization rates should become vanishingly small as E approaches the isomerization barrier height of ~43 kcal/mol (see Table 1). The fitted result is small but not small enough to result in F_H equaling the required value of 1, as seen

dx.doi.org/10.1021/jp3099889 | J. Phys. Chem. A XXXX, XXX, XXX−XXX

in Figure 7. At the high-energy end, a few tens of kcal/mol beyond the energy range of Figure 9, k_{ISO} begins to *decrease* with energy, a physically unlikely scenario.

Within the energy range of the trajectories, the fit is a close representation of the trajectory results as seen in Figure 4 but underestimates F_H as seen by the black curve in Figure 9 by $\leq$0.05. The majority of that underestimation is due to the use of statistical alternations that are shown in Figure 8 to underestimate trajectory results. However, at the higher energies, there is a residual underestimation of up to 0.02 that comes from an imperfect fit. As indicated at the beginning of this section, more elaborate kinetics models are possible that would further reduce fitting error. However, it is important to note that the fitting target was the evolution of the C_2H_5 population, not the H product population, with time. One could have fit the time dependent population of H from dissociation after each isomerization. Since F_H is all about products, it is likely such a fitting strategy would have improved agreement with trajectory calculations of F_H at some modest cost to representing trajectory populations after each isomerization.

5. CONCLUSIONS

Motivated by photodissociation experiments on the ethyl radical that have discovered very slow dissociation processes, we have performed a trajectory study of the dissociation and isomerization of C_2H_5 out to as much as 100 ps over an energy range of 100−150 kcal/mol. The feasible propagation of trajectories for such a long time requires an efficient model for the potential energy surface. In the first gas-phase application we are aware of, we used the AIREBO empirical molecular mechanics potential. In its native form, AIREBO has both technical and accuracy limitation in representing. However, a limited generalization of the potential energy form and a limited parameter optimization to select calculated CBS-QB3 saddle point properties for both dissociation and isomerization leads to a realistic AIREBO specific reaction parameter (SRP) surface appropriate for the unimolecular decay of C_2H_5. The resulting AIREBO-SRP surface largely retains the computational speed of the native AIREBO surfaces, allowing the feasible calculation of very long time trajectories.

At each energy, 10 000 trajectories were followed until essentially all dissociated. This is an order of magnitude longer in time and larger in sample size than any previous study. The trajectory results show no evidence of a very slow dissociation process. They do show evidence of multiexponential decay at the higher end of the energy range, but the rate constant components of this decay are still many orders of magnitude faster than slow decay observed and attributed to unimolecular processes on the ground state surface. The fraction of product energy deposited in translation is about 75% of the most recent measured value. Isotopic scrambling is overestimated for CD_2CH_3, with the fraction of products constituting H + CD_2H_2 calculated at about ~0.8, while the measured value is 0.95 ± 0.05. The alternation with repeated isomerization of the H fraction of products can be largely, but not completely, explained by an isomerization model.

A divided phase space kinetics model of dissociation and isomerization fits the trajectory results quite well. The divided phase space aspect of the model has one region of phase space that can isomerize/dissociate and a second region cannot. The IVR-like rate of transfer between those two regions relative to the dissociation and isomerization rate can influence product formation. The model represents the growth of multiexponential decay with increased energy, as seen in the trajectory results. The model represents in detail repeated isomerization processes. Interestingly, the model has isomerization and dissociation rates that vary relative to one another in a non-monotonic fashion as a function of energy, resulting in a H fraction of products that has a minimum with respect to energy. This suggests that precise measurements of the energy dependence of isotopic product fractions may reveal subtle aspects of the competition between isomerization and dissociation.

The AIREBO-SRP potential in this work bring to four the number of potential energy surfaces that have been used in trajectory studies relevant to photodissociation experiments. Only one of those potential energy surfaces[25] has produced "trapped trajectories" that indicate a slower process for ethyl radical dissociation. However, the actual value of the slower rate could not be determined because of the large sample error of the handful of trajectories involved and because of the very short times (~2 ps) the trajectories were followed. These results could be consistent with our trajectory results at higher energies that show multiexponential decay but with rates involved that are orders of magnitude different from the experimental observations. The authors of that study have noted the sensitivity of the trapping to details of the potential energy surface.[27] Every one of the four surfaces has been a compromise to higher-level descriptions in order to be computationally inexpensive enough to enable trajectory runs to the time scales necessary to make contact with experiment. From a theoretical perspective, any further dynamics studies would best be performed on a high fidelity fit to a high-level electronic structure description of the ground state potential energy surface. With 15 internal degrees of freedom, this is a challenging task, especially up to the energies sampled by the photodissociation experiments. We have been interested in the interpolated moving least-square (IMLS) method[43] of fitting potential energy surfaces automatically with a minimization of the number of electronics structure calculations that can be performed. Fitting the C_2H_5 surface with this method or other methods capable of automatic potential energy generation is a direction we intend to pursue for future research.

AUTHOR INFORMATION

Corresponding Author

*E-mail: thompsondon@missouri.edu. Phone: (573) 882-0051.

Notes

The authors declare no competing financial interest.

ACKNOWLEDGMENTS

We are grateful to Steven J. Stuart for providing us with the 2010 version of the AIREBO code and helpful suggestions on using it. We acknowledge helpful discussions with Branko Ruscic (Argonne National Laboratory) concerning the thermodynamics of the ethyl radical. This work was supported by the U.S. Department of Energy, Office of Basic Energy Sciences, Division of Chemical Sciences, Geosciences, and Biosciences under Contract No. DE-AC02-06CH11357 (Argonne) and by the U.S. Army Research Office Grant No. W911NF-09-1-0199.

GLOSSARY

AIREBO: adaptive intermolecular reactive empirical bond-order
CBS: complete basis set
CBS-QB3: complete basis set-quadratic Becke3
CCSD(T): coupled cluster with single, double, and perturbative triple
$C_i(t)$: population in region 2 of the ith isomer
DFT: density functional theory
F_1: phase space volume for region 1
F_2: phase space volume for region 2, $F_2 = 1 - F_1$
F_H: fraction H atom dissociation
$\langle f_T \rangle$: fraction of product energy released into translation
HCTH147@6-31+G**/6-31G**: HCTH147@6-31+G** density functional parametrized by Boese et al.[44] with the 6-31G** basis set
IMLS: interpolating moving least square
IVR: intramolecular vibrational redistribution
k_{12}: rate of trajectories hop from region 1 to region 2
k_{21}: rate of trajectories hop from region 2 to region 1
k_{DIS}: dissociation rate
k_{ISO}: isomerization rate
LJ: Lennard-Jones
M05-2X/CBSB7: M05-2X density functional described in ref 33 with the CBSB7 basis set; the CBSB7 has the form 6-311G(2d,d,p) used by the CBS-QB3 method[45]
MR-CISD: multireference configuration interaction with singles and doubles
PES: potential energy surface
$P_i(t)$: time-dependent normalized population
PM6: parametric method number 6
POL-CI: polarization configuration interaction
QCISD(T): quadratic configuration interaction with single, double, and perturbative triple
$Q_i(t)$: population in region 1 of the ith isomer
REBO: reactive empirical bond-order
RMS: root mean square
RRKM: Rice−Ramsperger−Kassel−Marcus
SA-MCSCF: state-averaged multiconfiguration self-consistent field
SEMO: semi-empirical molecular orbital
SRP: specific reaction parameters

REFERENCES

(1) Miller, J. A. Theory and Modeling in Combustion Chemistry. *Proc. Combust. Inst.* **1996**, *26*, 461−480.
(2) Miller, J. A.; Kee, R. J.; Westbrook, C. K. Chemical Kinetics and Combustion Modeling. *Annu. Rev. Phys. Chem.* **1990**, *41*, 345−387.
(3) The NIST Chemical Kinetics Database on the Web (http://kinetics.nist.gov/kinetics/) shows 35 entries going back to 1960. The earliest work goes back to: Rice, F. O. Elementary Organic Reactions. *J. Am. Chem. Soc.* **1934**, *56*, 488−490.
(4) Curran, H. J. Rate Constant Estimation for C_1 to C_4 Alkyl and Alkoxyl Radical Decomposition. *Int. J. Chem. Kinet.* **2006**, *38*, 250−275.
(5) Baulch, D. L.; Cobos, C. J.; Cox, R. A.; Frank, P.; Hayman, G.; Just, Th.; Kerr, J. A.; Murrells, T.; Pilling, M. J.; Troe, J.; et al. Evaluated Kinetic Data for Combustion Modeling. Supplement I. *J. Phys. Chem. Ref. Data* **1994**, *23*, 847−1033.
(6) Tsang, W.; Hampson, R. F. Chemical Kinetic Data Base for Combustion Chemistry. Part I. Methane and Related Compounds. *J. Phys. Chem. Ref. Data* **1986**, *15*, 1087−1279.
(7) Miller, J. A.; Klippenstein, S. J. The H + C_2H_2 (+M) → C_2H_3 (+M) and H + C_2H_2 (+M) → C_2H_5 (+M) Reactions: Electronic Structure, Variational Transition-State Theory, and Solutions to a Two-Dimensional Master Equation. *Phys. Chem. Chem. Phys.* **2004**, *6*, 1192−1202.
(8) Gilbert, T.; Gerbner, T. L.; Fischer, I.; Chen, P. Microcanonical Rates for the Unimolecular Dissociation of the Ethyl Radical. *J. Chem. Phys.* **1999**, *110*, 5485−5488.
(9) Amaral, G.; Xu, K.; Zhang, J. UV Photodissociation Dynamics of Ethyl Radical via the $^2A'(3s)$ State. *J. Chem. Phys.* **2001**, *114*, 5164−5169.
(10) Zierhut, M.; Noller, B.; Schultz, T.; Fischer, I. Excited-State Decay of Hydrocarbon Radicals, Investigated by Femtosecond Time-Resolved Photoionization: Ethyl, Propargyl, and Benzyl. *J. Chem. Phys.* **2005**, *122*, 094302.
(11) Steinbauer, M.; Giegerich, J.; Fischer, K. H.; Fischer, I. The Photodissociation Dynamics of the Ethyl Radical, C_2H_5, Investigated by Velocity Map Imaging. *J. Chem. Phys.* **2012**, *137*, 014303.
(12) Min, Z.; Quandt, R.; Bersohn, R. Kinetic Energies of Hydrogen Atoms Photodissociated from Alkyl Radicals. *Chem. Phys. Lett.* **1998**, *296*, 372−376.
(13) Brum, J. L.; Deshmukh, S.; Koplitz, B. Conclusive Evidence for Site-Specific C-H Bond Cleavage Resulting from 248 nm Photolysis of the Ethyl Radical. *J. Chem. Phys.* **1991**, *95*, 2200−2202; Iodoethane Photolysis: Which C-H Bond Leads to H-atom Formation? *J. Chem. Phys.* **1990**, *93*, 7504−7505.
(14) Zyubin, A. S.; Mebel, A. M.; Lin, S. H. Ab Initio Study of H Photodetachment from the Ethyl Radical. *Chem. Phys. Lett.* **2000**, *323*, 441−447.
(15) Weber, K. H.; Lemieux, J. M.; Zhang, J. Flash Pyrolysis of Ethyl, *n*-Propyl, and Isopropyl Iodides as Monitored by Supersonic Expansion Vacuum Ultraviolet Photoionization Time-of-Flight Mass Spectrometry. *J. Phys. Chem. A* **2009**, *113*, 583−591.
(16) Gordon, A. S.; Tardy, D. C.; Ireton, R. Ethyl Radical Isomerization. A 1,2-Hydrogen (Deuterium) Shift in the Pyrolysis of 1,1,1-trideuterioethane. *J. Phys. Chem.* **1976**, *80*, 1400−1404.
(17) Hase, W. L.; Mrowka, G.; Brudzynski, R. J.; Sloane, C. S. An Analytic Function Describing the H + C_2H_4 → C_2H_5 Potential Energy Surface. *J. Chem. Phys.* **1978**, *69*, 3548−3562.
(18) Hase, W. L.; Wolf, R. J.; Sloane, C. S. Trajectory Studies of the Molecular Dynamics of Ethyl Radical Decomposition. *J. Chem. Phys.* **1979**, *71*, 2911−2928. Hase, W. L.; Buckowski, D. G. Dynamics of Ethyl Radical Decomposition. II. Applicability of Classical Mechanics to Large-Molecule Unimolecular Reaction Dynamics. *J. Comput. Chem.* **1982**, *3*, 335−343.
(19) Hase, W. L.; Buckowski, D. G.; Swamy, K. N. Dynamics of Ethyl Radical Decomposition. 3. Effect of Chemical Activation vs. Microcanonical Sampling. *J. Phys. Chem.* **1983**, *87*, 2754−2763.
(20) Swamy, K. N.; Hase, W. L. A Quasiclassical Trajectory Calculation of the H + C_2H_4 → C_2H_5 Bimolecular Rate Constant. *J. Phys. Chem.* **1983**, *87*, 4715−4720.
(21) Hase, W. L.; Schlegel, H. B.; Balbyshev, V.; Page, M. An ab Initio Study of the Transition State and Forward and Reverse Rate Constants for C_2H_5 → H + C_2H_4. *J. Phys. Chem.* **1996**, *100*, 5354−5361.
(22) East, A. L. L.; Bunker, P. R. An ab Initio Calculation of the Rotation and Internal-Rotation Energy Levels of the Ethyl Radical. *Chem. Phys. Lett.* **1998**, *282*, 49−53.
(23) López-Ciudad, T.; Ramírez, R.; Schulte, J.; Böhm, M. C. Anharmonic Effects on the Structural and Vibrational Properties of the Ethyl Radical: A Path Integral Monte Carlo Study. *J. Chem. Phys.* **2003**, *119*, 4328−4338.
(24) Harding, L. B. Ab Initio Studies of (1,2)-Hydrogen Migrations in Open-Shell Hydrocarbons: Vinyl Radical, Ethyl Radical, and Triplet Methylcarbene. *J. Am. Chem. Soc.* **1981**, *103*, 7469−7475.
(25) Bach, A.; Hostettler, J. M.; Chen, P. Quasiperiodic Trajectories in the Unimolecular Dissociation of Ethyl Radicals by Time-Frequency Analysis. *J. Chem. Phys.* **2005**, *123*, 021101.
(26) Bach, A.; Hostettler, J. M.; Chen, P. Nonstatistical Effects in the Dissociation of Ethyl Radical: Finding Order in Chaos. *J. Chem. Phys.* **2006**, *125*, 024304.

dx.doi.org/10.1021/jp3099889 | J. Phys. Chem. A XXXX, XXX, XXX−XXX

(27) Hostettler, J. M.; Bach, A.; Chen, P. Adiabatic and Nonadiabatic Dissociation of Ethyl Radical. *J. Chem. Phys.* **2009**, *130*, 034303.
(28) See, e.g.: Torrence, C.; Compo, G. P. A Practical Guide to Wavelet Analysis. *Bull. Am. Meteorol. Soc.* **1998**, *79*, 61−78.
(29) Ruscic, B. Private communication of a result obtained from Active Thermochemical Tables (ATcT): (a) Ruscic, B.; Pinzon, R. E.; Morton, M. L.; von Laszevski, G.; Bittner, S. J.; Nijsure, S. G.; Amin, K. A.; Minkoff, M.; Wagner, A. F. Introduction to Active Thermochemical Tables: Several "Key" Enthalpies of Formation Revisited. *J. Phys. Chem. A* **2004**, *108*, 9979−9997. (b) Ruscic, B.; Pinzon, R. E.; von Laszewski, G.; Kodeboyina, D.; Burcat, A.; Leahy, D.; Montoy, D.; Wagner, A. F. Active Thermochemical Tables: Thermochemistry for the 21st Century. *J. Phys.: Conf. Ser.* **2005**, *16*, 561−570. ATcT requires a thermochemical network that came from: (c) Stevens, W. R.; Ruscic, B.; Baer, T. Heats of Formation of $C_6H_5^{\bullet}$, $C_6H_5^+$, and C_6H_5NO by Threshold Photoelectron Photoion Coincidence and Active Thermochemical Tables Analysis. *J. Phys. Chem. A* **2010**, *114*, 13134−13145. (d) Dixon-Lewis, G.; Marshall, P.; Ruscic, B.; Burcat, A.; Goos, E.; Cuoci, A.; Frassoldati, A.; Faravelli, T.; Glarborg, P. Inhibition of Hydrogen Oxidation by HBr and Br_2. *Combust. Flame* **2012**, *159*, 528−540. (e) Sivaramakrishnan, R.; Michael, J. V.; Ruscic, B. High-Temperature Rate Constants for H/D + C_2H_6 and C_3H_8. *Int. J. Chem. Kinet.* **2012**, *44*, 194−205.
(30) For the zero point energy corrections for C_2H_4: Martin, J. M. L.; Taylor, P. R. The Geometry, Vibrational Frequencies, and Total Atomization Energy of Ethylene. A Calibration Study. *Chem. Phys. Lett.* **1996**, *248*, 336−344. For C_2H_5, Ruscic, B. Private communication.
(31) The energetics are found in the Supporting Information of ref 25.
(32) Stewart, J. J. P. Optimization of Parameters for Semiempirical Methods V: Modification of NDDO Approximations and Application to 70 Elements. *J. Mol. Model.* **2007**, *13*, 1173−1213.
(33) Zhao, Y.; Schultz, N. E.; Truhlar, D. G. Design of Density Functionals by Combining the Method of Constraint Satisfaction with Parametrization for Thermochemistry, Thermochemical Kinetics, and Noncovalent Interactions. *J. Chem. Theory Comput.* **2006**, *2*, 364−382.
(34) Stuart, S. J.; Tutein, A. B.; Harrison, J. A. A Reactive Potential for Hydrocarbons with Intermolecular Interactions. *J. Chem. Phys.* **2000**, *112*, 6472−6486.
(35) Liu, A.; Stuart, S. J. Empirical Bond-Order Potential for Hydrocarbon: Adaptive Treatment of van der Waals Interactions. *J. Comput. Chem.* **2008**, *29*, 601−611.
(36) Private communication (2010) with Steven J. Stuart. The version of the AIREBO code we received contained elements described in refs 34 and 35 with an improved algorithm to reduce computation cost.
(37) Yan, T.; Doubleday, C.; Hase, W. L. A PM3-SRP + Analytic Function Potential Energy Surface Model for $O(^3P)$ Reactions with Alkanes. Applications to $O(^3P)$ + Ethane. *J. Phys. Chem. A* **2004**, *108*, 9863−9875.
(38) Dybala-Defratyka, A.; Paneth, P.; Pu, J.; Truhlar, D. G. Benchmark Results for Hydrogen Atom Transfer between Carbon Centers and Validation of Electronic Structure Methods for Bond Energies and Barrier Heights. *J. Phys. Chem. A* **2004**, *108*, 2475−2486.
(39) A transcription error in the CBS-QB3 dissociation barrier height and tunneling frequency resulted in an AIREBO-SRP PES that matched slightly incorrect values. The barrier height matched is 40.3 kcal/mol rather than the value of 40.5 kcal/mol as now listed in Table 1. The frequency matched is −367 cm^{-1} rather than −308 cm^{-1} as now listed in Table 3. This error was discovered after all the calculations were completed. This is a small imperfection that we believe does not alter the conclusions of this study.
(40) A version based on GENDYN (http://www.chem.missouri.edu/Thompson/research/gendyn.htm) was used to calculate the trajectories.
(41) The Markov walk was performed using a version of efficient microcanonical sampling (EMS): (a) Nyman, G.; Rynefors, K.; Holmlid, L. Efficient Microcanonical Sampling for Triatomic Molecular Systems: Exact Distribution Verified. *J. Chem. Phys.* **1988**, *88*, 3571−3580. (b) Nyman, G.; Nordholm, S.; Schranz, H. W. Efficient Microcanonical Sampling for a Preselected Total Angular Momentum. *J. Chem. Phys.* **1990**, *93*, 6767−6773. (c) Schranz, H. W.; Nordholm, S.; Nyman, G. An Efficient Microcanonical Sampling Procedure for Molecular System. *J. Chem. Phys.* **1991**, *94*, 1487−1498.
(42) The distance increment was selected after preliminary trajectory runs on the AIREBO PES produced results no different from results with the same trajectories propagated with the analytic gradients of AIREBO. Unfortunately, the SRP changes in AIREBO-SRP require redoing the analytic gradients, which we did not attempt.
(43) Dawes, R.; Wagner, A. F.; Thompson, D. L. Ab Initio Wavenumber Accurate Spectroscopy: $^1CH_2$ and HCN Vibrational Levels on Automatically Generated IMLS Potential Energy Surfaces. *J. Phys. Chem. A* **2009**, *113*, 4709−4721.
(44) Boese, A. D.; Martin, J. M. L.; Handy, N. C. The Role of the Basis Set: Assessing Density Functional Theory. *J. Chem. Phys.* **2003**, *119*, 3005−3014.
(45) Montgomery, J. A.; Frisch, M. J.; Ocheterski, J. W.; Petersson, G. A. A Complete Basis Set Model Chemistry. VI. Use of Density Functional Geometries and Frequencies. *J. Chem. Phys.* **1999**, *110*, 2822−2827.